

Select Topics in Mass Transfer and Magnetic Braking

by

Kenny Van

A thesis submitted in partial fulfillment of the requirements for the degree of

Master of Science

Department of Physics
University of Alberta

© Kenny Van, 2017

Abstract

In this thesis we investigate a novel binary formation channel with a semi-degenerate donor and examine the stability criteria in binary systems with a massive donor. First we will review the current basics in the understanding of binary systems along with where recent research has been moving in this area. Following this we will review the implementation of these theories in the binary evolution code used throughout the rest of the thesis. We then apply this code to a novel binary formation scenario involving a black hole and a semi-degenerate donor. The key difference in this formation channel and previous work is the amount lost during dynamical encounter. Following this we investigate the stability of mass transfer in massive donors. We find that should the onset of mass transfer occur between two key points of instability in a massive star's evolution, the mass transfer in the system is stable. This has dramatic effects on the formation rate of possible black hole-black hole mergers and may instead be a possible formation channel for ultra luminous X-ray sources. Finally we go over the assumptions made in this work and how these affect the reliability of the results presented.

Preface

This thesis is an original work by Kenny Van in collaboration with Professor Natalia Ivanova and Professor Craig Heinke at the University of Alberta. It is based substantially on the following papers: Pavlovskii et al. (2017) and Ivanova et al. (2017).

The work described in Chapter 3 was used in Ivanova et al. (2017). I was responsible for running and analyzing the 1D **MESA** simulations used in this work. Coauthors Cassio and Jose were responsible for the 3D SPH simulations. Professor Ivanova was the primary author of the theoretical concept.

The improvements to mass transfer rate described in Section 1.4.1 were created by Konstantin Pavlovskii as detailed in Pavlovskii and Ivanova (2015). The improved mass transfer prescription was adapted from the version of **MESA** used by Konstantin in Pavlovskii and Ivanova (2015) to a newer version by me.

The work described in Chapter 4 was used in Pavlovskii et al. (2017). The improved mass transfer prescription that was imported to a newer version of **MESA** was used in this work. Both Konstantin and I were responsible for the simulations used in the work. The analysis of the resulting binaries was done by Professor Ivanova and Konstantin while the population synthesis analysis was done by Professor Belczynski.

“It is not necessary to have a physically correct expression in order to obtain sensible answers”

Peter P. Eggleton

Acknowledgements

First and foremost I would like to thank my supervisor, Professor Natalia Ivanova for the guidance and help. Without her this thesis would not have been possible. I would also like to thank the entire University of Alberta astrophysics group who have provided support through the entire graduate program.

I would also like to thank the `MESA` support group and in particular Bill Paxton and Pablo Marchant who created the `MESA` code and the binary prescriptions within. Without their help and the existence of the `MESA` software this research would have been substantially more difficult.

Finally, I would like to thank my family and friends for the support they provided through the entire process.

Contents

1	Introduction	1
1.1	Importance of Binary Systems	1
1.2	Importance of Mass Transfer	2
1.2.1	Mass Transfer Stability	5
1.3	Importance of Angular Momentum Loss	7
1.3.1	Gravitational Radiation	8
1.3.2	Magnetic Braking	9
1.3.3	Angular Momentum Loss Through Mass Loss	10
1.4	Current Advancements	11
1.4.1	Improvements to Mass Transfer	11
1.4.2	Improvements In Angular Momentum Loss	12
1.4.3	Areas of Ongoing Research	14
2	Methods	16
2.1	MESA Code	16
2.1.1	MESA Implementations of Mass Transfer	16
2.1.2	Implicit and Explicit Mass Transfer	19
2.1.3	Stability of Mass Transfer	21
2.1.4	MESA Implementations of Angular Momentum Loss	22
2.2	Additions Implemented in MESA	25
2.2.1	Mass Transfer Additions	26
2.2.2	Changes to Eddington Limit	27

2.2.3	Additions to Magnetic Braking	29
3	Envelope Stripping	32
3.1	Introduction	32
3.2	Stripping Method	33
3.2.1	Caveats and Problems	34
3.3	Applications and Results	38
4	Stability of Mass Transfer in High Mass Donors	42
4.1	Introduction	42
4.2	Stability Criteria	43
4.3	Binary Simulations	44
4.4	Results	46
4.4.1	Ultra Luminous X-Ray Sources	47
4.5	Applications	48
5	Reliability of Current Prescriptions	51
5.1	Reliability of Roche Lobe Mass Transfer	51
5.2	Reliability of Magnetic Braking	53
6	Summary and Conclusions	57
A	Custom MESA Routines	72
A.1	Implementation of Eddington Limit	72
A.2	Implementation of Magnetic Braking	73
B	Sample MESA <i>inlist</i> Files	77
B.1	Relaxation Sample	77

List of Tables

4.1 Critical Radii For Mass Transfer Stability.	45
---	----

List of Figures

1.1	Roche lobe schematic in the x-y plane with a $1.4M_{\odot}$ accretor and a $1.0M_{\odot}$ donor, initial separation of $26R_{\odot}$. The two curves represent two different surfaces of gravitational equipotential. If the donor star radius exceeds the smaller grey lobe, then mass will be lost through the L_1 point. If the donor overfills beyond the dashed curve then it will lose mass through the L_2 point.	4
2.1	A simple comparison of the affects of limiting the time step and changing tolerances on the smoothness of evolutionary tracks. The system modelled with a $1.4M_{\odot}$ point source accretor and a $1.1M_{\odot}$ donor initially placed at a 2.2 day period.	22
2.2	A comparison between the Eddington limit described by Equations 2.9 and 2.10. The dashed line is Equation 2.9 is the Eddington limit for Black holes. The full line is Equation 2.10 which is the Eddington limit for Neutron stars assuming $R_a = 11.5\text{km}$. The system being tested is a $1.0M_{\odot}$ donor with a $1.3M_{\odot}$ accretor with an initial period of 7.59 days.	28
2.3	An example of how using a optical depth limit and velocity ratio limit can change the resulting turnover time. The star tested here is a $1 M_{\odot}$ star evolved to near solar age to show oscillations in the turnover time.	30

3.1	The entropy profiles of a $Z = 0.01$, $1 M_{\odot}$ star at $2 R_{\odot}$ prior to fast mass loss represented in the black line and after losing mass at a variety of mass loss rates. The cyan line shows the highest mass transfer rate we could achieve in MESA . The three lower mass transfer rates show how an entropy profile can readjust. . .	35
3.2	The change in radius of the donor star as it is quickly stripped of mass. The vertical black line represents the point where we stop the fast mass loss and place the donor in a binary system. . .	37
3.3	A plot comparing the evolution of the $1M_{\odot}$ star if it remained unperturbed, evolved as a single star after stripping and as a stripped star in a binary system. The black solid line shows the evolutionary track of a $1M_{\odot}$ star without stripping. The position of the $1M_{\odot}$ and $2R_{\odot}$ subgiant prior to the stripping is indicated with the red circle. The location of the stripped star immediately after the stripping down to $0.3M_{\odot}$ is indicated with the blue circle. The black dashed line shows the evolution of the stripped star as a single star. Tracks with the colors show the evolution of the stripped star in a binary system. The colors of the tracks indicate instantaneous characteristic timescales, such that it takes to change either the magnitude M V by one or color BV by 0.2. The initial orbital periods are $P_{\text{orb}} = 0.21, 0.54, 0.97$ and 1.46 days.	39
3.4	The same plot as Figure 3.3 but instead with the case of stripping the donor down to $0.4M_{\odot}$ with initial periods of $P_{\text{orb}} = 0.32, 0.88, 1.62$ and 2.48 days.	40
3.5	The same plot as Figure 3.3 but instead with the case of stripping the donor down to $0.5M_{\odot}$ with initial periods of $P_{\text{orb}} = 0.42, 1.98, 4.22$ and 6.95 days.	41

4.1 A sample of the mass transfer in a binary with a $20 M_{\odot}$ giant and a $7 M_{\odot}$ black hole. The gaps in the evolution track are when the donor detaches. The figure is taken from Pavlovskii et al. (2017).	48
4.2 A time averaged distribution of ULXs formed in the simulations using conservative mass transfer are given in the red. The observed distributions of ULXs within 5 Mpc are shown in the hatched area (Gladstone et al., 2013). The figure is taken from Pavlovskii et al. (2017)	50

Chapter 1

Introduction

From the initial suggestion by Michell (1767) that stars may interact with one another to the recent advancements in observatories and modelling techniques, our understanding of stellar and binary evolution has drastically changed. Despite the improvements mentioned, many outstanding issues still exist within our understanding of these systems. Ranging from uncertainties with the formation rate of the systems themselves to the properties of the system during evolution, many of these issues remain topics of research in the field. In this work, we will go over some underlying theory for binary systems and how they interact. We will then explain how these theories are applied in the stellar code **MESA** in Chapter 2. In Chapters 3 and 4, applications of the theories and **MESA** code will be discussed. Chapter 5 will reiterate uncertainties with how the theories were applied in this work and how these uncertainties may affect the results.

1.1 Importance of Binary Systems

Initially introduced by Herschel (1802) in his catalogue, a binary system is a system where two stars are gravitationally bound to one another and thus, orbit about a center of mass. While over 200 years have passed since the first

discovery of these systems, we still do not have a comprehensive understanding of how stars evolve in binary systems. The impact of a companion star on stellar evolution is not minor; many stars exist in systems with a companion (Abt and Levy, 1976; Duchêne and Kraus, 2013; Mason et al., 1998). A large fraction of these systems in binaries are expected to interact at some point during their lifetime (Kobulnicky et al., 2012, 2014; Sana et al., 2012). With such a large fraction of stars predicted to interact, it is suggestive the phenomena observed in stars is heavily influenced by binarity. These phenomena range from blue stragglers (Bailyn, 1995), where mass transfer causes the accretor to appear bluer and younger, to the recent detection of gravitational wave emissions from binary black hole systems (Abbott et al., 2016a,b, 2017).

1.2 Importance of Mass Transfer

The evolution of a binary system is greatly influenced by interactions between the two stars. While it is possible a binary may be formed with a large enough binary separation where the two stars only interact gravitationally, if the two stars are close enough together, the stars will undergo mass transfer at some point in their evolution. This transfer of mass from one star to the other results in X-ray radiation being emitted as mass is accreted if the accretor is compact. These systems are known as X-ray binaries. Depending on binary properties such as the distance between the two stars, the donor's mass and it's evolutionary state, the accretion process may be wind fed or through what we will call L_1 mass transfer. The onset of L_1 mass transfer occurs when a star overfills its Roche lobe.

The Roche lobe of a star is the region where the material is still gravitationally bound to it. If the radius of the star exceeds the Roche lobe of the given star, the material may then be transferred to the companion or simply lost from the system. The Roche potential, assuming a circular orbit, constant

angular velocity and a corotating frame with the binary is given by:

$$\Phi_{RL}(x, y, z) = -\frac{GM_d}{\sqrt{[x+(M_a/M)a]^2+y^2+z^2}} - \frac{GM_a}{\sqrt{[x-(M_d/M)a]^2+y^2+z^2}} - \frac{GM}{2a^3}(x^2 + y^2) \quad (1.1)$$

Equation 1.1 is adapted from Eggleton (2006) where G is the gravitational constant. M_d and M_a are the masses of the donor and accretor respectively. From this point onwards, the subscripts d and a denote the donor and accretor respectively. M is the combined mass of the two stars and a is the separation between the two stars. The above equation is represented in Cartesian coordinates (x, y, z) where the origin is located at the center of mass of the binary. A graphical representation of Equation 1.1 is shown in Figure 1.1. The various coloured lines show surfaces of gravitational equipotential. A neutral point exists where the equipotential surface crosses over itself, this is known as the inner Lagrange or L_1 Lagrange point. This is the point of first intersection between the accretor and donor Roche lobes and where material will begin to flow through during mass transfer. This process where the donor radius exceeds the Roche lobe and results in matter flowing across L_1 is known as Roche lobe overflow (RLOF) and is the primary method of mass transfer.

The radius of the Roche lobe crossing through the L_1 point can be approximated by (Eggleton, 1983)

$$\frac{R_{RL}}{a} \approx \frac{0.49q^{2/3}}{0.6q^{2/3} + \ln(1 + q^{1/3})}, \quad (1.2)$$

where R_{RL} represents the radius of the Roche lobe and q is the mass ratio M_d/M_a . From this approximation there are three classes of close binaries as described by Kopal (1955):

1. Detached Systems: Neither star fills their respective Roche lobe and the stars interact gravitationally. The stars may still transfer mass through

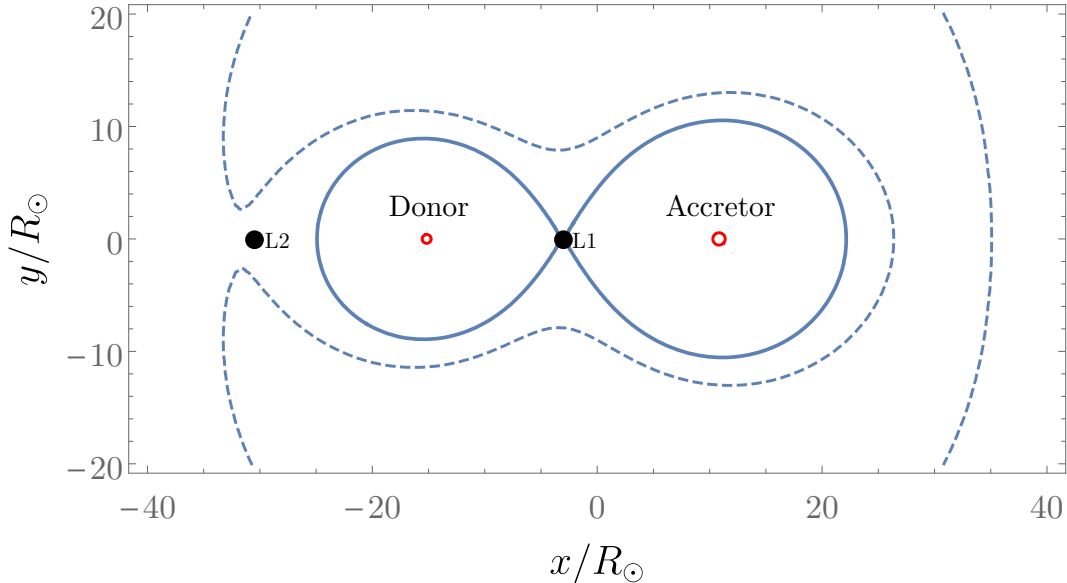


Figure 1.1: Roche lobe schematic in the x - y plane with a $1.4M_\odot$ accretor and a $1.0M_\odot$ donor, initial separation of $26R_\odot$. The two curves represent two different surfaces of gravitational equipotential. If the donor star radius exceeds the smaller grey lobe, then mass will be lost through the L_1 point. If the donor overfills beyond the dashed curve then it will lose mass through the L_2 point.

winds but no mass is transferred through the L_1 point.

2. Semi-detached Systems: One of the stars fills its Roche lobe allowing for mass transfer to occur through the L_1 point from the donor to the accretor.
3. Contact Systems: Both stars fill their respective Roche lobes and the stars are in physical contact with one another.

A fourth possibility exists where the donor star overfills the L_2 point. The matter flowing through the L_2 will either leave the system entirely or remain bound to the system resulting in what is known as common envelope evolution (Paczynski, 1976). In this scenario, the two stars are so close together they orbit within a shared common envelope. The details of this scenario are a topic of ongoing research and are outside the scope of this work (see Ivanova

et al., 2013, for a review on common envelope events). In this work, we will focus on semi-detached systems where RLOF occurs.

1.2.1 Mass Transfer Stability

Once mass transfer begins, the timescale at which the process occurs is directly linked to its stability and lifetime. Stability depends on how the donor and accretor respond to mass transfer and how the Roche lobe changes over the course of evolution (Hjellming and Webbink, 1987; Soberman et al., 1997). The stability of mass transfer in binary systems is generally defined by three mass-radius exponents

$$\xi_{\text{eq}} = \left(\frac{d \ln R}{d \ln M} \right)_{\text{eq}}, \quad \xi_{\text{RL}} = \left(\frac{d \ln R}{d \ln M} \right)_{\text{RL}}, \quad \xi_{\text{ad}} = \left(\frac{d \ln R}{d \ln M} \right)_{\text{ad}}, \quad (1.3)$$

which define the mass-radius exponents for stars in thermal equilibrium, the Roche lobe of the star, and for the star losing mass adiabatically. Based on these three mass-radius exponents, there are three different mass transfer cases corresponding to three different timescales.

1. Stable mass transfer occurs when $\xi_{\text{RL}} \leq \xi_{\text{eq}}$. This corresponds to the case where the donor star remains in thermal equilibrium and thus does not expand quickly. The mass transfer is driven by nuclear evolution of the donor and occurs on the nuclear timescale. For example, in the case of a main sequence star it is

$$\tau_{\text{nuc}} \approx 10^{10} \frac{M}{M_{\odot}} \frac{L_{\odot}}{L} \text{yr} \quad (1.4)$$

2. The mass transfer in the next step up is thermal timescale mass transfer. In this regime $\xi_{\text{ad}} \geq \xi_{\text{RL}} > \xi_{\text{eq}}$ and mass transfer is driven by thermal readjustment of the donor star. The thermal mass transfer rate can start

as low as $\approx 10^{-8} M_{\odot}\text{yr}^{-1}$ for a Sun-like $1M_{\odot}$ star transferring to a $1.4M_{\odot}$ Neutron star. This mass transfer is still dynamically stable and self-regulating. If mass transfer is too low, then the donor star will expand to force the mass transfer rate to the appropriate value. If the mass transfer is too large, then the donor star will shrink within its Roche lobe reducing the mass transfer rate.

3. The case where mass transfer is dynamically unstable is when $\xi_{\text{RL}} > \xi_{\text{ad}}$. This mass transfer occurs on a short timescale and the star cannot readjust quickly enough to shrink the radius to keep it within the Roche lobe. The response of the donor star in these cases is tied to the entropy profile of the star. If the entropy profile of the star is constant with respect to the mass coordinate of the star, the star will experience expansion as it loses mass. This results in the radius of the donor continuously expanding causing the mass transfer rate to also continuously grow. It has been shown however in the work of Woods and Ivanova (2011) and Pavlovskii and Ivanova (2015) the response of the donor star differs from the simplified approach in Hjellming and Webbink (1987). The donor may not be continuously expanding as the surface of the star may be able to readjust. Systems with high mass transfers which overfill the L_2 point are expected to undergo a common envelope event and spiral in phase (see Ivanova et al., 2013; Ivanova and Nandez, 2016, for more details on common envelope events and the spiral in phase). Recent work by Pavlovskii et al. (2017) has shown if mass transfer occurs within a stability range, even if the system overfills the L_2 point it will not experience unstable mass transfer. See Chapter 4 for more information on this stability range.

These three types of mass transfer can generally describe the stability of the system. Beyond this simple classification of stability, it is also possible for mass

transfer to be initially stable, increase over the course of the system’s evolution, and lead to a delayed dynamical instability (see Webbink, 1985; Hjellming and Webbink, 1987, for more details on this instability). This delayed instability occurs in stars that initially have a deep radiative envelope and are stable to short timescale mass transfer. As the mass of the envelope is stripped away however, the entropy gradient of the star may flatten. Should the star be stripped to a point where the entropy profile is flat with increasing mass, the star will experience expansion as described in the dynamically unstable case.

Dynamically unstable mass transfer is commonly calculated using an adiabatic approximation. Adiabatic mass loss does not exist in nature and is a result of assumptions made in modelling mass transfer (Hjellming and Webbink, 1987). If the mass transfer rate occurs on timescales where thermal readjustment cannot occur the entropy of the star does not have sufficient time to readjust and react to the mass loss. Due to the entropy of the star being unable to readjust, the stability of mass transfer will be overestimated in stars with a radiative envelope and underestimated in stars with a convective envelope (Ge et al., 2015). The details of adiabatic mass transfer are still a topic of ongoing research and as such we will be using the simplified three classifications of mass transfer (see Ge et al., 2010, 2015; Woods and Ivanova, 2011, and the references therein for more details on the stability of adiabatic mass transfer).

1.3 Importance of Angular Momentum Loss

Mass transfer is the most visible method of binary interaction but the donor star must fill its Roche lobe for this to occur. This normally occurs in one of two ways, the donor star expands over the course of its evolution or the Roche lobe of the star shrinks. Stellar expansion occurs naturally and the radius of the star can increase by orders of magnitude once it leaves the main sequence. Binary separation decreasing prior to this point in stellar evolution is also expected as

there is evidence of stellar interaction during the main sequence (Sana et al., 2012). From Equation 1.2, we see the radius of the Roche lobe depends on two factors: the mass ratio of the system and the binary separation. Before mass transfer can occur, the changes in the mass ratio should not appreciably change the size of the Roche lobes. Instead, what normally drives the Roche lobes to shrink is a decrease in the binary separation of the stars. Equation 1.5 describes the relationship between angular momentum J , binary separation, the masses of the system and the eccentricity e of the orbit.

$$J^2 = G \frac{M_d^2 M_a^2}{M_d + M_a} a(1 - e^2), \quad (1.5)$$

$$2 \frac{\dot{J}}{J} = \frac{\dot{a}}{a} + 2 \frac{\dot{M}_d}{M_d} + 2 \frac{\dot{M}_a}{M_a} - \frac{\dot{M}_d + \dot{M}_a}{M_d + M_a} - 2 \frac{\dot{e}e}{1 - e^2}. \quad (1.6)$$

From Equation 1.6, we see the primary method of bringing the two stars in a circular orbit closer together without losing mass is through the loss of angular momentum.

1.3.1 Gravitational Radiation

Perhaps the most well understood mechanism of angular momentum loss is gravitational radiation, the process where angular momentum of the system is lost through the emission of gravitational waves. With the canonical example of how accurate the predictions of gravitational radiation are being the Hulse-Taylor Binary (Weisberg and Taylor, 2005). The loss of angular momentum, assuming a circular orbit is described by (Kraft et al., 1962; Landau and Lifshitz, 1975)

$$\frac{\dot{J}_{GR}}{J} = -\frac{32G^3}{5c^5} \frac{M_d M_a (M_d + M_a)}{a^4}, \quad (1.7)$$

$$\tau_{\text{GR}} = \frac{-J}{\dot{J}_{\text{GR}}} = \frac{5c^5}{32G^3} \frac{a^4}{M_d M_a (M_d + M_a)}, \quad (1.8)$$

τ_{GR} describes the timescale for angular momentum loss through gravitational radiation. Gravitational radiation only comes into play when the binaries are already very close together as it scales with a^4 . As an example, for a system similar to the one shown in Figure 1.1 with a $1.0M_\odot$ donor and a $1.4M_\odot$ accretor requires a separation $a \lesssim 2.5R_\odot$ for τ_{GR} to be comparable to Hubble time.

1.3.2 Magnetic Braking

While gravitational radiation dominates in very close binaries, magnetic braking is important even in systems where the separation is large. Magnetic braking is the process where mass being lost from the star via stellar winds is still bound to the star due to magnetic field of the star. Despite the amount of mass being relatively small, the radius where the material is locked to the star's surface rotation is large. This results in an appreciable amount of angular momentum being lost when this mass leaves the system.

Unlike gravitational radiation which was derived from field equations (Kraft et al., 1962; Landau and Lifshitz, 1975), the current default equation for magnetic braking was derived from observations (Skumanich, 1972). As such, the default prescription for magnetic braking which is commonly referred to as the Skumanich magnetic braking law, is calibrated to work with a specific subset of stellar systems. Skumanich initially calibrated the rate of angular momentum loss to single G type main sequence stars. The equation can be written more generally from Rappaport et al. (1983):

$$\dot{J}_{\text{MB,Sk}} = -3.8 \times 10^{-30} M_d R_d^4 \left(\frac{R_d}{R_\odot} \right)^{\gamma_{\text{mb}}} \Omega^3 \text{ dyne cm} \quad (1.9)$$

Here, M_d and R_d are the mass and radius of the donor, while γ_{mb} is a dimensionless parameter normally ranging from 0 to 4, although there has

been work where γ_{mb} has been as large as 5 (Istrate et al., 2014; Sengar et al., 2017). $\gamma_{\text{mb}} = 4$ corresponds to the Skumanich scaling for magnetic braking. Ω is the angular velocity of the donor in units of s^{-1} .

1.3.3 Angular Momentum Loss Through Mass Loss

Once the separation between the two stars has decreased to the point where the donor star can fill its Roche lobe, mass transfer can occur. Just as mass transfer may be stable or unstable as classified in Section 1.2, it can also be conservative or non-conservative.

Conservative mass transfer is the case where the total mass of the binary is conserved. This means $\dot{M}_d + \dot{M}_a = 0$, thus all of the mass lost from the donor is accreted onto the companion star. In most cases, conservative mass transfer can represent an upper limit for the possible increase in mass for the accretor. More importantly, it is not expected that conservative mass transfer will hold in many circumstances.

Non-conservative mass transfer, on the other hand, is the case where the total mass of the binary is not conserved $\dot{M}_d + \dot{M}_a \neq 0$. Mass is lost from the system through mechanisms such as wind and limits in mass transfer. It is argued the accretion rate is likely limited by the Eddington limit. The Eddington limit is where gravitational force pulling material onto the companion is balanced by the radiative force from the energy being released by the accretion. It is often assumed a mass transfer rate above the Eddington limit results in a fraction of the mass transferred being lost from the system with the specific angular momentum of the accretor. The mass lost through the wind of the star carries the specific angular momentum of the star where the wind originated. It is important to note it is possible for accretion to exceed the Eddington limit and super-Eddington accretion is thought to be a possibility for the formation of ultra-luminous X-ray sources (Colbert and Mushotzky, 1999).

1.4 Current Advancements

In case of both mass loss and angular momentum loss, the current prescriptions used to describe the effects of these processes are not complete. The two phenomena are connected in binary systems and in general, must be studied together.

1.4.1 Improvements to Mass Transfer

In this work, we will be using an improved prescription of mass transfer developed by Pavlovskii and Ivanova (2015). This mass transfer prescription will be used in Chapter 4 where the stability of mass transfer is uncertain. The key features of this mass transfer scheme are the following:

- A more detailed treatment of the outer super-adiabatic layer. Specifically, it was found the donor star does not experience an aggressive expansion predicted by adiabatic considerations, resulting in more stable mass transfer.
- The use of detailed geometry in calculating the nozzle size at the L_1 Lagrange point and the use of optically thick flow of matter. Consideration of a non-instantaneous mass removal, but of a stream determined by conditions in the L_1 neighbourhood allows for stability at higher mass transfer rates.

An important point to make is a star is not required to remain within its Roche lobe. In addition to these mass transfer changes, two additional criteria for mass transfer stability are given in Pavlovskii and Ivanova (2015).

- If the donor star does not overfill its Roche lobe to the point of L_2 overflow, the system is expected to be stable. This criterion has been confirmed by three-dimensional simulations where overflow of the L_2 point

quickly leads to a common envelope event (Nandez et al., 2014) or a circumbinary disk. It is important to note simulations that have experienced L_2 overflow result in dynamically unstable mass transfer and a subsequent common envelope event. Observed binary systems such as SS 433 have been found to remain stable after this overflow (Bowler, 2010; Perez M. and Blundell, 2010; Pavlovskii and Ivanova, 2015).

- Or, if the parameters of the binary orbit are changing rapidly, this may invalidate the Roche formalism. The Roche formalism requires the centrifugal term in calculating the Roche potential be much larger than the Coriolis term, which is ignored in the formalism. If parameters such as the angular velocity change substantially during evolution, the Coriolis term becomes comparable to the centrifugal term causing the formalism to break down (Sepinsky et al., 2007).

1.4.2 Improvements In Angular Momentum Loss

Improvements made to the angular momentum loss in this work will be done through modifications in the magnetic braking prescription. These changes to magnetic braking will only be used in future work.

The most commonly used form of Equation 1.9 used in calculations of low-mass X-ray binaries is known as the Skumanich Law. The standard Skumanich Law is using Equation 1.9 with $\gamma_{\text{mb}} = 4$. The Skumanich law corresponds to the form of the magnetic braking that best matches the observed spin down of main sequence G type stars.

The magnetic braking however, can depend on the wind mass loss in donor stars, as it is not the same as the wind mass loss for the main sequence G type stars, on which the original magnetic braking was calibrated. In addition, the strength of a dynamo-generated magnetic field may depend on the convective eddies turnover time τ_{conv} (see discussion in Ivanova, 2006). We use the pre-

scription described in Pavlovskii and Ivanova (2015) that takes into account these two effects:

$$\dot{\mathbf{j}}_{\text{MB,boost}} = \frac{\dot{M}_d^w}{\dot{M}_\odot} \left(\frac{\tau_{\text{conv}}}{\tau_{\odot\text{conv}}} \right)^\zeta \dot{\mathbf{j}}_{\text{MB,sk}} \quad (1.10)$$

This magnetic braking prescription has two additional scaling factors.

- \dot{M}_d^w is the wind mass loss rate of the donor star. The wind mass loss is related to the amount of mass corotating with the star through the magnetic fields. In Equation 1.10, this value is scaled with the wind mass loss of the Sun. This results in systems with super-solar wind mass loss having boosted magnetic braking. Conversely, systems with sub-solar wind mass loss rates have a damped magnetic braking.
- τ_{conv} is the turnover time of convective eddies found as following:

$$\tau_{\text{conv}} = \int_R^{R_s} \frac{dr}{v_{\text{conv}}}, \quad (1.11)$$

R and R_s are the bottom and the top of the outer convective zone respectively, while v_{conv} is the local convective velocity. The convective turnover time is related to the strength of the magnetic field. The magnetic activity of the star scales with N_D the dynamo number (Hinata, 1989; Meunier et al., 1997; Parker, 1971). The dynamo number in turn, scales with the convective turnover time in the form $N_D \sim (\Omega \tau_{\text{conv}})^2$ (Noyes et al., 1984).

The power ζ can vary, where $\zeta = 2$ describes the same simplified assumptions for which Skumanich law is valid (i.e., radial magnetic field and isothermal winds). ζ might be as high as 4, for the case, of giant's winds, where velocity of winds grows linearly with distance; we note though in this case, the dependence on the angular velocity also has to be modified to become a power 5.

In the case of relatively fast rotating stars, about 10 times faster than the Sun, it is argued the strength of the magnetic braking is weaker if compared

to the standard Skumanich law. Indeed, in the case of a fast rotating star, the magnetic field is no longer radial within the Alfvén zone. Wind is then trapped within the so-called “dead” zones and is not able to leave the star reducing the loss of angular momentum (Ivanova and Taam, 2003). For stars rotating at $\Omega > 10 \Omega_{\odot}$, we adopt the scaling

$$\dot{J}_{MB,sat} = \dot{J}_{MB,boost} \times \frac{\Omega^{1.3} (10 \Omega_{\odot})^{1.7}}{(10 \Omega_{\odot})^3} \quad (1.12)$$

1.4.3 Areas of Ongoing Research

The mass transfer description given here is a simplified version of what happens in nature. Woods and Ivanova (2011) looked at stability of mass transfer and how adiabatic approximations effect this stability. Stability of mass transfer to the so called delayed dynamical instability (Webbink, 1985; Hjellming and Webbink, 1987) is also a topic of ongoing research. A change in the parameter space where mass transfer is stable or unstable can greatly change the expected results from binary evolution. With a greater number of unstable systems, we would expect more instances of common envelope evolution or mergers.

Beyond the criteria for stability being researched, the physics of the accretion itself are not well understood. Due to the angular momentum of the system, it is likely the flow of material from the donor to accretor forms an accretion disc. The exact physics of the disc are an ongoing topic of research and can affect how much mass will be accreted (see Lasota, 2007, 2016, for more information on the physics of accretion discs.). In addition to the stability of mass transfer being uncertain, the stability of the accretion disc itself is an area of ongoing research (see Lasota, 2001, for a review of disc instability models). The stability of an accretion disc results in systems falling into two categories of X-ray binaries, persistent and transient systems (Meyer and Meyer-Hofmeister, 1981). In cases where the accretion disc is stable, the accretion disc does not experience outbursts and is therefore persistent. Systems

which have an unstable accretion disc will undergo outbursts resulting in large fluctuations in luminosity (Lasota, 2001; Coriat et al., 2012).

As explained in Section 1.3, gravitational radiation is well understood but angular momentum loss through mass loss and magnetic braking are areas of research. For massive stars where wind mass loss rates are most uncertain, the rate by which the system loses angular momentum is poorly constrained (Renzo et al., 2017). Magnetic braking, which plays a large role in lower mass systems, is most uncertain in the magnetic field configuration, coupling with the wind, and internal structure of stars for more massive systems. Currently, there are different magnetic braking prescriptions being calibrated to work with different systems. Examples of these magnetic braking schemes include Chen and Podsiadlowski (2016) and Justham et al. (2006) which were created for Ap/Bp stars, Ivanova and Taam (2003) which was designed for rapidly rotating main sequence stars, Ivanova (2006) for pre-main sequence stars, and Pavlovskii and Ivanova (2016) which was created for stars that have evolved beyond the main sequence. These magnetic braking schemes are calibrated for specific models and may not be applicable in dramatically different systems. Therefore, it is possible through the evolution of a system, different magnetic braking schemes may be more or less valid at different points. Without a more unified scheme that transitions well from one prescription to another, there will be errors in the amount of angular momentum lost.

Chapter 2

Methods

2.1 MESA Code

All calculations for the single stars and for mass transferring binaries in this work were performed using the one-dimensional stellar evolution code **MESA**¹ (Modules for Experiments in Stellar Astrophysics) revision 7736 in Chapter 4 and revision 8677 in the subsequent Chapters. **MESA** is a modern open source set of stellar libraries as described in Paxton et al. (2011, 2013, 2015).

In this chapter, I will go over the implementations of mass transfer and magnetic braking in **MESA** with a focus on the limitations of these prescriptions. I will then explain the additions made to **MESA** in this work and where these additions were applied in the work. Due to the frequency of **MESA** updates, the descriptions presented in this chapter are for revisions 8677 unless explicitly stated.

2.1.1 MESA Implementations of Mass Transfer

Within the default **MESA** package, there are three mass transfer schemes within revision 8677. The effectiveness and use cases for the three schemes differ and

¹<http://mesa.sourceforge.net>

will be described below. In the current revision of **MESA** at the time of writing, release 9575 includes a fourth mass transfer method used for contact binaries (Marchant et al., 2016).

Ritter

Initially created by Ritter (1988) to model short-period semi-detached binaries with a low mass companion, and designed to work in the case where $R_d \leq R_{RL}$. This mass transfer prescription assumes the donor star will fill its Roche volume and transfer mass through the L_1 Lagrange point. This scheme applies an exponential scaling factor to calculate the mass flow and is implemented within **MESA** with the following set of equations:

$$\begin{aligned}\dot{M}_{\text{ritter}} &= -\frac{2\pi}{\sqrt{e}} \left(\frac{k_b T_d}{\mu m_p} \right)^{3/2} \frac{R_{RL}^3}{GM_d} \rho_d F_1 e^{\gamma_{\text{ritter}}} \\ \gamma_{\text{ritter}} &= -\gamma \left(\frac{R_{RL} - R_d}{H_p} \right)\end{aligned}\quad (2.1)$$

$$F_1 = 1.23 + 0.5 \log(q_a), \quad 0.5 \leq q_a \leq 10$$

$$\gamma = \begin{cases} 0.954 + 0.025 \log(q_a) - 0.038 \log(q_a)^2, & 0.04 \lesssim q_a \lesssim 1 \\ 0.954 + 0.039 \log(q_a) + 0.114 \log(q_a)^2, & 1 \lesssim q_a \lesssim 20 \end{cases}$$

With $q_a = \frac{M_a}{M_d}$, this differs from $q = \frac{M_d}{M_a}$, e being Euler's constant, k_b the Boltzmann constant and proton mass m_p . μ is the mean molecular weight, T is the temperature and H_p is the pressure scale height. It is important to note the pressure scale height used in the Ritter mass transfer equations is a modified pressure scale height and is different from the normal pressure scale height. F_1 and γ are two fitting functions where $1.07 \leq F_1 \leq 1.73$ and $\gamma \sim 1$. For the exact details on how this is derived, see Ritter (1988) and Mochnacki (1984).

This scheme was designed for optically thin flow where $R_d \leq R_{RL}$. However, mass transfer continues to points where $R_d < R_{RL}$. In **MESA**, the Ritter scheme

continues to calculate mass transfer rates when $R_d > R_{RL}$. In the cases where q is outside the ranges given in Equations 2.1, the mass transfer rate is calculated using F_1 and γ at the edge of the respective boundary.

Kolb

The “Kolb” scheme builds upon the theories presented in Ritter (1988). Where the Ritter scheme was designed for optically thin flow, the Kolb scheme was expanded to explicitly include optically thick flow as well. Just as optically thin flow is described as $R_d \leq R_{RL}$, optically thick flow is the inverse, $R_d > R_{RL}$. The additional treatment of optically thick flow in the Kolb theory is calculated in MESA by:

$$\dot{M}_{kolb} = 2\pi F_1 \frac{R_{RL}^3}{GM_d} \int_{P_{ph}}^{P_{RL}} \left(\frac{2}{\Gamma_1 + 1} \right)^{\frac{\Gamma_1 + 1}{2(\Gamma_1 - 1)}} \Gamma_1^{1/2} \sqrt{\frac{k_b T_d}{m_p \mu}} dP \quad (2.2)$$

Where the variables are the same as described in Equation 2.1, Γ_1 is the adiabatic coefficient, P is the pressure where the subscripts RL and ph denote the Roche lobe and the photosphere respectively.

The optically thick term in the Kolb method does not play a significant role on the mass transfer rate as long as the following conditions are met:

1. The mass transfer rate is sensitive to the difference between the radius of the donor and the radius of the Roche lobe.
2. The pressure scale height of the outer layers of the donor star is small compared to the radius of the star.
3. The change in radius of the Roche lobe and donor star are similar.

The optically thick term does not play a large role in our calculations as our models satisfy all three of the above conditions. Due to the additional term

that must be calculated in the Kolb method, the computational cost of this prescription is greater than that of the Ritter prescription while resulting in insignificant changes to mass transfer. Therefore, in this work we will be using the Ritter prescription for mass transfer.

Roche_Lobe

The Roche_Lobe method does not calculate mass transfer rate based on the properties of the star. Instead, this mass transfer method will adjust a mass transfer rate such that $R_d = R_{RL}$ or in other words, the mass transfer is constrained so the radius of the star is exactly the radius of the Roche lobe. It is not practical to constrain that the two values are numerically the same, instead, they are calculated to within a tolerance value.

$$f(\dot{M}_{RLOF}) = \frac{2(R_d - R_{RL})}{R_{RL}} + \xi_{\text{implicit}} \quad (2.3)$$

Here ξ_{implicit} is some tolerance value input by the user. Should $f < -\xi_{\text{implicit}}$ then the mass transfer rate is set to zero and the binary is assumed to have detached. Different values of ξ_{implicit} can result in quite different solutions (Paxton et al., 2015). As this mass transfer scheme is not motivated by the properties and instead created to keep the donor within its Roche lobe, we will not be using this mass transfer scheme.

2.1.2 Implicit and Explicit Mass Transfer

The above mass transfer schemes describe the equations used to calculate the amount of mass transferred with given properties of the donor. Computationally however, the calculations are done in discrete time steps and this results in discrete changes to the stellar model instead of a continuous evolution. Due to this, the mass transfer rate can be calculated at one of two points, at the beginning of the time step or at the end of the time step. The case where the

calculation is done at the beginning of the time step is known as “explicit”. Conversely, “implicit” mass transfer is the case where the calculation is iterated until it satisfies a “convergence” condition at the end of the time step. Both Ritter and Kolb methods prescriptions of mass transfer can be either implicit or explicit, while the Roche_Lobe method can only be implicit. Both the implicit and explicit calculations contain a smoothing parameter used to suppress large oscillations that may arise. For explicit mass transfer:

$$\dot{M}_s = \dot{M}_i \xi_{\text{explicit}} + (1 - \xi_{\text{explicit}}) \dot{M} \quad (2.4)$$

where ξ_{explicit} is some value between 0 and 1 affecting the averaging between the mass transfer rate in the previous step \dot{M}_i and the current mass transfer rate \dot{M} to produce a smoothed mass value \dot{M}_s . If $\xi_{\text{explicit}} = 0$ there is no smoothing applied.

For implicit mass transfer:

$$\left| \frac{\dot{M}_s - \dot{M}_f}{\dot{M}_f} \right| < \xi_{\text{implicit}} \quad (2.5)$$

Equation 2.5 is only used if the Ritter or Kolb scheme is being used implicitly and will iterate the calculation. In the case where the Roche_Lobe scheme is being applied, Equation 2.3 is used instead. Similar to Equation 2.4, \dot{M}_s is the smoothed mass transfer value while \dot{M} is the mass transfer rate calculated at the end of the step.

An important distinction between the explicit and implicit methods can be seen when we compare Equations 2.4 and 2.5. The explicit method takes an average value but the implicit method requires numerical iteration to achieve the condition given in Equation 2.5.

2.1.3 Stability of Mass Transfer

Equations 2.4 and 2.5 both attempt to smooth out any numeric oscillations that can appear but using “good” values for the ξ values in either equation is an exercise in trial and error. For better or worse, **MESA** is a robust code that does everything it can to avoid crashing. As a result, despite the user’s best efforts, it is possible for numeric noise to dominate results. **MESA** will reduce time step size until the solver within the code can converge on a result. This reduction in time step directly leads to numerical oscillations, as with short enough time steps any smoothing applied through the evolution is on a tiny scale and lost. If the numerical noise is greater than the change in time step, the models will still converge but the solution will be incorrect. In cases where **MESA** quickly converges on a solution, the solver will increase the time step size, possibly speeding up the simulation time. A caveat with large time steps is the possibility of too much smoothing in the results. Should the time step be too large or the smoothing be too aggressive it is likely that finer changes in the properties of the star will be lost.

Within **MESA** there are “tolerance” options pertaining to numerical convergence which define what the solver determines as “converged”. A larger residual means the solver is less likely to force a reduction in time step as convergence can be reached more easily. In theory, this should result in fewer oscillations but in practice, things are less monotonic. The user must also be cautious in allowing the code to move towards time steps that wash out finer details in the evolution. While it is possible to set an upper limit to how large a time step the code may use, similar to ξ or the options defining convergence, it is not a simple task to determine a “best” value.

A simple example of how the mass transfer type, tolerances and maximum time steps change the smoothness of the calculated mass transfer rate is shown in Figure 2.1. The figure does not have numbers on the y-axis as this is meant to only show the general shape of the curves. With the imposed offset on

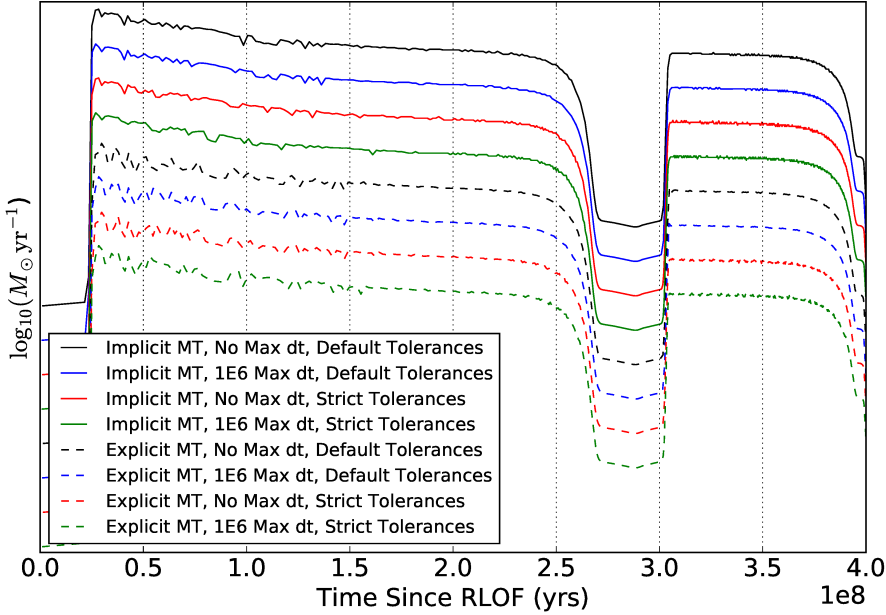


Figure 2.1: A simple comparison of the affects of limiting the time step and changing tolerances on the smoothness of evolutionary tracks. The system modelled with a $1.4M_{\odot}$ point source accretor and a $1.1M_{\odot}$ donor initially placed at a 2.2 day period.

each subsequent curve, numerical values in the y-axis would not be useful. It is important to note however that the maximum mass transfer rate in this example system is $\approx 10^{-8}M_{\odot}\text{yr}^{-1}$. From this simple comparison, the explicit mass transfer rate experiences larger oscillations than the implicit calculation but the implicit method encounters more oscillations as visible in the later portions of the evolution. The effects of the tolerances and time step limitations is more visible in the right half of the curve where we can see more numerical noise appearing when these parameters are used.

2.1.4 MESA Implementations of Angular Momentum Loss

The models described in Chapters 3 and 4 lose angular momentum through gravitational radiation, mass loss and magnetic braking.

$$\dot{J}_{\text{orb}} = \dot{J}_{\text{GR}} + \dot{J}_{\text{ml}} + \dot{J}_{\text{MB}} \quad (2.6)$$

Gravitational Radiation

As mentioned in Section 1.3.2, gravitational radiation is likely the most well understood form of angular momentum loss. Within `MESA`, it is implemented in the same form as Equation 1.7.

Mass Loss

Mass can be lost from stars in a variety methods. The forms of mass loss can range from tidal stripping removing large amount of mass from a star to non-conservative mass transfer slowly removing mass. An example of an event removing large amounts of mass is the fast mass loss we apply in Chapter 3 to create a semi-degenerate donor. This mass would carry significant angular momentum from the system were it removed. Beyond this case in Chapter 3, the majority of mass loss in this work will primarily be through stellar winds and non-conservative mass transfer. Mass loss due to non-conservative mass transfer is described by:

$$\dot{J}_{\text{ML}} = \dot{M}_{\text{d,ejected}} \left(\frac{M_{\text{d}}}{M_{\text{d}} + M_{\text{a}}} a \right)^2 \Omega + \dot{M}_{\text{a,ejected}} \left(\frac{M_{\text{a}}}{M_{\text{d}} + M_{\text{a}}} a \right)^2 \Omega \quad (2.7)$$

In this work our donor star does not accrete any material. This results in the mass being ejected from the donor star to be entirely through winds, $\dot{M}_{\text{d,ejected}} = \dot{M}_{\text{d,w}}$. The mass that is lost through the donor wind $\dot{M}_{\text{d,w}}$ leaves the system with angular momentum of the donor. While the mass that is transferred non-conservatively is given by $\dot{M}_{\text{a,ejected}} = \dot{M}_{\text{d,L}_1} - \dot{M}_{\text{accreted}}$. In the case where accretion rate is equal to the Eddington limit, $\dot{M}_{\text{accreted}} = \dot{M}_{\text{Edd}}$, and the excess mass flowing through the L_1 point that is beyond the Eddington limit carries

angular momentum of the accretor.

In principle if the accretor also loses mass through wind then an additional $\dot{M}_{a,w}$ would be included in $\dot{M}_{a,ejected}$. Uncertainties in the wind mass loss scheme used will result in differences in amount of angular momentum losses (see Renzo et al., 2017, for a thorough study of uncertainties in wind prescriptions for massive stars within **MESA**). The other key source of uncertainty in Equation 2.7 is using an appropriate Eddington mass accretion limit. An incorrect limit results in large differences in mass transfer, see Section 2.2.2 for changes implemented to **MESA** to properly calculate the Eddington limit in our case.

An alternative method in calculating mass loss from the system is the usage of “efficiency” parameters (Soberman et al., 1997; Tauris and van den Heuvel, 2006). The amount of mass that is transferred in this case is denoted by $\epsilon = 1 - \alpha - \beta - \delta$. Here ϵ represents the amount of mass transferred while α , β , and δ correspond to the fraction of mass lost near the donor, the accretor and through a circumbinary toroid respectively. In the case where the mass transfer is completely conservative $\epsilon = 1$ and $\alpha = \beta = \delta$.

Both implementations of non-conservative mass transfer can be used within **MESA**. We will not be using the α , β , δ calculation and instead, only calculate mass loss through Equation 2.7. This is because the efficiency parameters are less physically motivated. We instead will allow non-conservative mass transfer to be driven by limits of accretion and wind mass loss.

Magnetic Braking

As explained in Section 1.3.2, the default prescription for magnetic braking is given by:

$$\dot{\mathbf{j}}_{MB,Sk} = -3.8 \times 10^{-30} M_d R_d^4 \left(\frac{R_d}{R_\odot} \right)^{\gamma_{mb}} \Omega^3 \text{ dyne cm}$$

while the default prescription is calibrated to G type main sequence stars,

it can be applied to a wider range of systems. It is important to note this magnetic braking scheme is expected to overestimate the angular momentum loss in rapidly rotating systems (Ivanova and Taam, 2003) and underestimate in cases where the donor has super-solar winds or a deep convective envelope (Pavlovskii and Ivanova, 2016).

The default magnetic braking is implemented within **MESA** as shown in Equation 1.9. The various stellar properties required to calculate the magnetic braking are taken from the donor star while the γ_{mb} parameter is supplied by the user as an initial condition. What is important to note is how the angular velocity of the star is calculated. **MESA** requires the stars to be in tidal synchronization to calculate magnetic braking. With this requirement, the angular velocity becomes $\Omega = \frac{2\pi}{P_{\text{orb}}}$ where P_{orb} is the orbital period of the binary. The resulting equation in **MESA** becomes:

$$\dot{J}_{\text{MB,Sk}} = -3.8 \times 10^{-30} M_d R_d^4 \left(\frac{R_d}{R_\odot} \right)^{\gamma_{\text{mb}}} \left(\frac{2\pi}{P_{\text{orb}}} \right)^3 \text{ dyne cm} \quad (2.8)$$

With the uncertainties in the formation and configuration of the magnetic field, we will assume should the star develop a fully convective core, no magnetic braking will take place, though magnetic braking may still exist in systems with convective cores.

2.2 Additions Implemented in MESA

Within this work we implement modifications to **MESA** in areas of mass transfer and magnetic braking. The changes to mass transfer were adapted from Pavlovskii and Ivanova (2015) with additional changes to the calculation of the Eddington limit. The changes to magnetic braking were adapted from Pavlovskii and Ivanova (2016) and Ivanova and Taam (2003).

2.2.1 Mass Transfer Additions

As explained in Section 1.4.1, the mass transfer prescription from Pavlovskii and Ivanova (2015) applies more detailed calculations in determining the effects of the superadiabatic layer. It was found the recombination energy in the superadiabatic layer plays a large role in determining the luminosity and effective temperature of the star. Additionally, acceleration near the surface is non-negligible and affects the pressure at the outer boundary of the star. These changes to the star result in changes in stability of mass transfer.

The other set of changes implemented to mass transfer rate are in the context of how to describe the geometry of the L_1 Lagrange point as well as the properties of the mass flowing through the nozzle. These improvements implemented can be summarized into key features:

- The geometry outside of the Roche lobe was explicitly calculated and tabulated. These calculations were done with higher order terms that play a large role in surfaces of equipotential far from the Roche lobe surface. These larger equipotentials are important for stars expanding with substantial RLOF.
- Pressure correspondence is not assumed in these calculations. Pressure correspondence is the assumption thermodynamic parameters at some point in 3D are identical to those in 1D if the pressure at these two points are equal. This assumption cannot be made if mass transfer is high.
- Neither the donor nor the matter flowing through is assumed to be polytropic. Instead flow is assumed to be adiabatic and instead uses equations of state from within `MESA` to calculate the mixing and radiative pressure.

It is crucial to note all of these changes were implemented with `MESA` revisions 7624. Unfortunately due to an overhaul of the treatment of hydrodynamic

terms in a subsequent update we have not been able to port the mass transfer changes to recent revisions of the code.

2.2.2 Changes to Eddington Limit

While not directly related to the calculation of the mass transfer rate, the Eddington limit controls the amount of mass that may be accreted. Within MESA the default calculation for the Eddington limit is:

$$\dot{M}_{\text{Edd}} = \frac{4\pi GM_a}{c\kappa_e}. \quad (2.9)$$

Where G is the gravitational constant, c is the speed of light and κ_e is the opacity. In our work, we will use the opacity due to Thomson electron scattering $\kappa_e = 0.2(X + 1)\text{cm}^2\text{g}^{-1}$, where X is the hydrogen mass fraction in the matter being transferred. This Eddington limit assumes that the matter is converted into radiation via $L_x = \epsilon \dot{M}_d c^2$, with ϵ being an efficiency value. The prescription given in Equation 2.9 only applies to black holes and assumes that the material being accreted onto the black hole is converted to radiation with perfect efficiency. It is not possible for the matter to be converted into radiation with perfect efficiency and a different equation should be used. If the system uses a neutron star instead a different prescription is required. The luminosity is calculated using $L_x = \frac{GM_d \dot{M}_d}{R_d}$, the Eddington limit we use for neutron stars is:

$$\dot{M}_{\text{Edd}} = \frac{4\pi c R_a}{\kappa_e} \approx \frac{3.4}{1+X} \times 10^{-8} M_{\odot} \text{yr}^{-1} \quad (2.10)$$

We assume $R_a = 11.5$ km as the radius of the neutron star ². It is important to note Equation 2.10 will also work for black holes with $R_a = R_{\text{ISCO}}$, where R_{ISCO} is the radius of the innermost stable circular orbit. An additional efficiency

²Exact code used for implementation of this Eddington limit is in Section A.1.

value may also be applied to Equation 2.10.

Different Eddington limit prescriptions have drastic effects to the end result in binary systems if the mass transfer rate is high. A comparison between the two Eddington limits is shown in Figure 2.2. The system being tested is a binary with a $1.0 M_{\odot}$ donor and a $1.3 M_{\odot}$ accretor with an initial period of 7.59 days. We can see with a change in Eddington limit the accretor grows by a much larger amount. The final mass of the accretor using Equation 2.9 is $1.73 M_{\odot}$ and the accretor using Equation 2.10 is $1.35 M_{\odot}$.

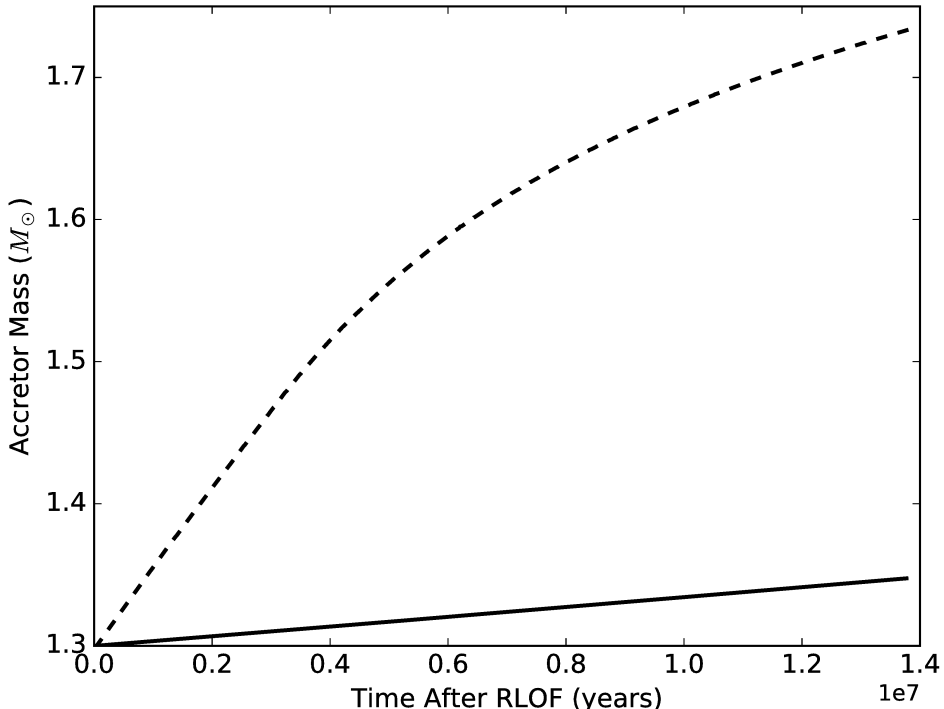


Figure 2.2: A comparison between the Eddington limit described by Equations 2.9 and 2.10. The dashed line is Equation 2.9 is the Eddington limit for Black holes. The full line is Equation 2.10 which is the Eddington limit for Neutron stars assuming $R_a = 11.5\text{km}$. The system being tested is a $1.0M_{\odot}$ donor with a $1.3M_{\odot}$ accretor with an initial period of 7.59 days.

2.2.3 Additions to Magnetic Braking

The default magnetic braking scheme used was calibrated for single sun-like stars. This prescription is not expected to work well for binaries or for more evolved stars. To try to improve the magnetic braking prescription we implement the theoretical changes suggested by Pavlovskii and Ivanova (2016) and Ivanova and Taam (2003)³.

Additions From Pavlovskii and Ivanova (2016)

In the work of Pavlovskii and Ivanova (2016), they looked at how the wind mass loss rate and the convective turnover time can change the strength of magnetic braking. Magnetic braking can depend on the mass lost due to wind in the donor stars. This effect is especially apparent if the wind mass loss rate differs greatly from the wind mass loss rate from the Sun. The other source of scaling explored in Pavlovskii and Ivanova (2016) is how the strength of the dynamo-generated magnetic field can scale with the turnover timescale of the convective eddies.

This is implemented within MESA with Equation 1.10. To account for the solar wind scaling, we use a solar wind loss rate of $\dot{M}_\odot = 2.5 \times 10^{-14} \text{ M}_\odot \text{yr}^{-1}$ (Carroll and Ostlie, 2006). This translates to approximately $1.6 \times 10^{-12} \text{ gs}^{-1}$, which are the units MESA uses for wind mass loss rates within its calculations.

The convective turnover time τ_{conv} was found through a summation instead of an integral:

$$\tau_{\text{conv}} = \sum_{r=R}^{r=R_s} \frac{dr}{v_{\text{conv}}} \quad (2.11)$$

In principle, we should take the summation from R to R_s where these represent the bottom and surface of the outer convective zone respectively. v_{conv} is the

³Exact code used for implementation of the changes in magnetic braking can be found in Section A.2

convective velocity in the cell dr . In practice the convective velocity becomes very small near the surface of the convective zone and dominates the calculation. This results in large jumps in the turnover time that dominate the result. To alleviate this issue, we require the outer boundary of the convective zone be defined at the optical depth of 1 and the ratio between convective velocity and the sound speed is small $\frac{v_{\text{conv}}}{v_{\text{sound}}} > 0.001$.

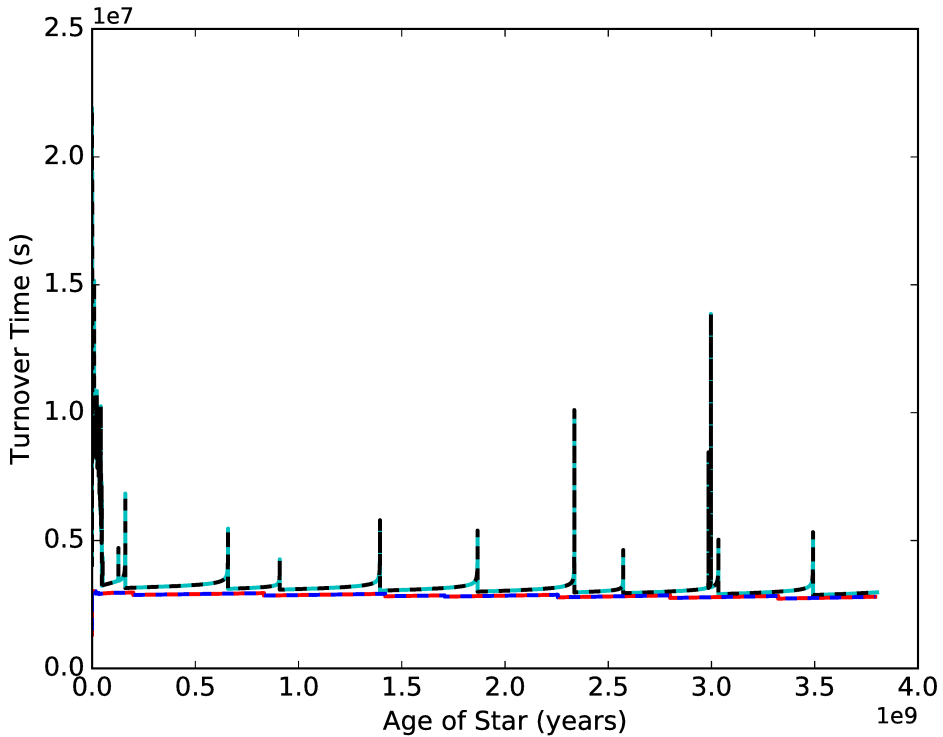


Figure 2.3: An example of how using a optical depth limit and velocity ratio limit can change the resulting turnover time. The star tested here is a $1 M_\odot$ star evolved to near solar age to show oscillations in the turnover time.

Figure 2.3 shows how the optical depth limit and velocity ratio affect the resulting turnover time calculation. In the figure, the solid cyan and dashed black lines represent the two cases where there is no velocity ratio limiting. The cyan line does not have an optical depth limit while the black line has an optical depth limit of 1. The red line uses a velocity ratio of 0.001 and no optical depth limit. The dashed blue line uses both the velocity ratio of

0.001 and the optical depth limit of 1. From these four cases, we see requiring the velocity ratio to be small greatly reduces the numeric oscillations in the results. The optical depth on the other hand does not result in large changes. To remain self consistent, the solar convective turnover time $\tau_{\odot\text{conv}}$ was found by evolving a default $1M_{\odot}$ MESA model with $Z=0.020$ to 4.6 Gyrs. This results in $\tau_{\odot\text{conv}} = 2.8 \times 10^6$ s.

Rotation Saturation

The rotation rate of stars is calculated using $\Omega = \frac{2\pi}{P_{\text{rot}}}$ with P_{rot} being the period of rotation for the star. However, with tidal synchronization $P_{\text{rot}} = P_{\text{orb}}$ so the rotation period of the star is equal to the orbital period. From Ivanova and Taam (2003) and Section 1.4.2, when stars reach high rotation rates, the magnetic braking is expected to be damped. Using the threshold from Ivanova and Taam (2003) of $\Omega > 10 \Omega_{\odot}$, equation 1.12 becomes:

$$\dot{J}_{\text{MB,sat}} = J_{\text{MB,boost}} \times \left(\frac{2073600 \text{ s}}{10 P} \right)^{1.3} \quad (2.12)$$

With the solar orbital period of 24 days or 2073600 seconds. $\Omega > 10 \Omega_{\odot}$ when converted to period becomes $P < 2.4$ days. This will result in binaries with periods shorter than 2.4 days to have magnetic braking which scales as $\dot{J} \propto \Omega^{1.3}$ instead of the $\dot{J} \propto \Omega^3$ scaling found in slow rotators.

Chapter 3

Envelope Stripping

3.1 Introduction

Once a binary has been formed, the mass transfer can vary in stability and thus, vary in mass transfer rate. It is also reasonable to assume many binaries will circularize over the course of the evolution (Zahn and Bouchet, 1989). However, depending on how the binary system was formed, it is possible for a substantial amount of mass to be stripped from the donor star in a short period of time. Should the binary be formed through what is known as a tidal capture event, a large fraction of the donor star's envelope may be stripped off (Fabian et al., 1975).

In general, a tidal capture event occurs when a compact object and a donor star come close enough together that kinetic energy from the compact object is dumped into the donor star. This transfer of kinetic energy into the donor can result in the entirety of the envelope being stripped off or, if the encounter is close enough, a physical collision may occur (Bacon et al., 1996). However, if the compact object cannot dump enough energy into the donor star, the binary will not become bound.

In this chapter, we will be exploring dynamic formation channel of a binary system consisting of a black hole accretor and semi-degenerate donor. This

formation channel is novel in that it differs from the physical collision channel which has been previously studied (Bacon et al., 1996). The key difference lies in the amount of mass removed in the formation and in the physical collision channel, the entire envelope of the donor star is stripped resulting in a black hole with a degenerate donor. In the grazing case we explore, only a fraction of the mass is stripped from the donor resulting in a semi-degenerate donor.

3.2 Stripping Method

In nature, stripping of the envelope should occur on the order of days. Unfortunately, this type of change is difficult, if not impossible, to do in a 1D code such as **MESA**. Smoothed particle hydrodynamics codes such as **STARSMASHER** (Gaburov et al., 2010; Lombardi et al., 2011) can more easily strip stars, as such we will be using a SPH code to predict the amount of mass to be stripped off the donor. The evolution of the system post stripping must be done with **MESA** instead of **STARSMASHER** as SPH codes cannot evolve a star.

To model the envelope stripping due to the tidal encounter in a consistent way, a few steps must be taken:

1. Evolve a 1D single star to the specific evolutionary stage in isolation. In this work, we evolved a $1M_{\odot}$, $Z = 0.01$ star until it expanded to $2R_{\odot}$.
2. Apply a rapid mass loss rate to the single star to obtain a semi-degenerate donor with the same mass predicted by SPH simulations.
3. Place this stripped star in a binary system at the predicted binary separation. The binary separation was taken from the SPH simulations which resulted in the semi-degenerate donor.

3.2.1 Caveats and Problems

While the process of stripping and modelling the stripped star appears straightforward, there are a variety of caveats to consider.

- There are large uncertainties with initial parameters in the evolution, changing parameters such as overshooting and mixing can change the properties of the star. Depending on how these mixing terms are applied to the stellar model, the size of the convective core as well as the main sequence lifetime of the star may differ. With larger amounts of mixing, more fuel becomes available to the star during the main sequence extending the lifetime.
- Mass stripping occurs on a very small timescale which can translate to mass losses of $\approx 10M_{\odot} \text{ yr}^{-1}$. MESA cannot accommodate mass loss rates this high and instead, we forced a mass loss of $1M_{\odot} \text{ yr}^{-1}$. It is important to note the mass loss rate must be high enough the entropy profile of the star does not change over the course of the stripping.
- MESA does not have a mass transfer prescription in the case for eccentric binaries. As such, we will instead model the mass transfer at limiting cases and two intermediate cases to estimate how the stripped star may appear in this range. The limiting cases are taken from the SPH simulations where the shortest period case sets the binary separation as the distance at periastron. The largest binary separation used will be using a binary separation with the same semimajor axis as found in the SPH simulations.

Of these three primary problems, the issues with the high mass loss and freezing the entropy profile are the largest issues in mass stripping. In our case, as we use a $1.0M_{\odot}$ donor star in our simulations and force fast mass loss on the subgiant branch, the first caveat plays a smaller role than if our donor was

a high mass star. The lack of `MESA` being able to simulate an eccentric binary undergoing mass transfer may be alleviated by testing the limiting cases as mentioned above.

The $1M_{\odot} \text{ yr}^{-1}$ mass loss is sufficiently large such that the entropy profile of the donor star does not have sufficient time to readjust. A low-mass radiative layer appears at the surface after envelope stripping. The low radiative layer can be seen in Figure 3.1 in the cyan line. It is important to note the x coordinate in the figure is stellar mass and the radiative layer is thin in mass. Lower mass transfer rates are also shown in Figure 3.1 and mass transfer rates that are too low result in the entropy profile readjusting.

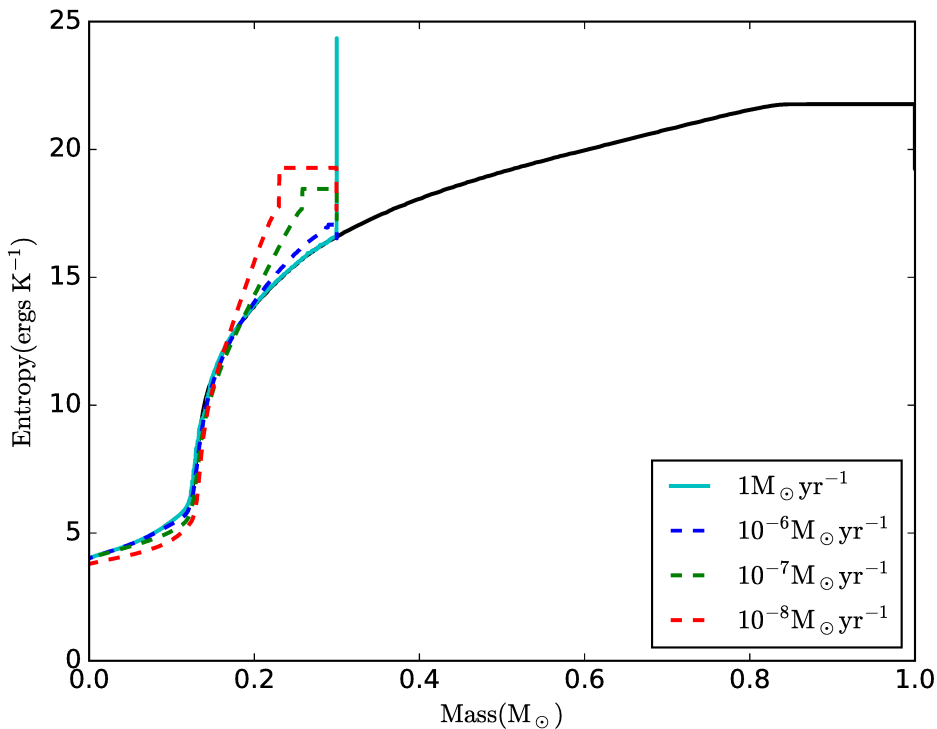


Figure 3.1: The entropy profiles of a $Z = 0.01$, $1 M_{\odot}$ star at $2 R_{\odot}$ prior to fast mass loss represented in the black line and after losing mass at a variety of mass loss rates. The cyan line shows the highest mass transfer rate we could achieve in `MESA`. The three lower mass transfer rates show how an entropy profile can readjust.

We could not evolve our star through fast mass loss without the appearance of a radiative layer. This outer radiative layer with mass $\leq 10^{-4}M_{\odot}$ causes the radius of our stripped star to be larger than expected. For comparison, the star shown in Figure 3.1 has a mass of $0.3M_{\odot}$ and radius of $0.47R_{\odot}$ after stripping. A similar star stripped with **STARSMASHER** has a radius of $0.32R_{\odot}$. Attempts at removing this radiative surface layer include using a much smaller time step prescription as well as changing possible surface atmosphere prescriptions.

Forcing the calculation to smaller time steps will normally lead to numeric issues if any physics occurs as the time steps shrink. To more safely force a small time step, the user must allow for a “relaxation” phase where minimal evolution occurs¹. Shrinking the time step still resulted in a thin radiative layer on the surface of the star. The small step size also caused numeric oscillations resulting in fluctuations in effective temperature and luminosity.

Various atmospheric boundary conditions are available in **MESA** which control how various properties such as pressure and temperature are calculated at the surface as well as where to do these calculations. Among the boundary conditions available, only a subset of them are theoretically valid for these studies (see Paxton et al., 2011, 2013, for more information on the various atmospheric boundary condition options.).

- “Simple Photosphere” is the default option where values of the atmosphere are estimated at an optical depth of $\tau = 2/3$.
- “Photosphere Tables” uses a set of precalculated tables within **MESA** for the photosphere.
- “Grey and Kap” uses a prescription where a simple grey atmosphere is calculated to find a consistent pressure, temperature and opacity at the surface.

¹See Section B.1 for a sample `inlist`.

- “Eddington Grey” integrates hydrostatic balance equations using the Eddington $T - \tau$ relation (Eddington, 1926).

These four atmospheric conditions resulted in different properties in the star but in all cases, the radiative surface layer persisted and the star had a larger radius than expected from the 3D simulations.

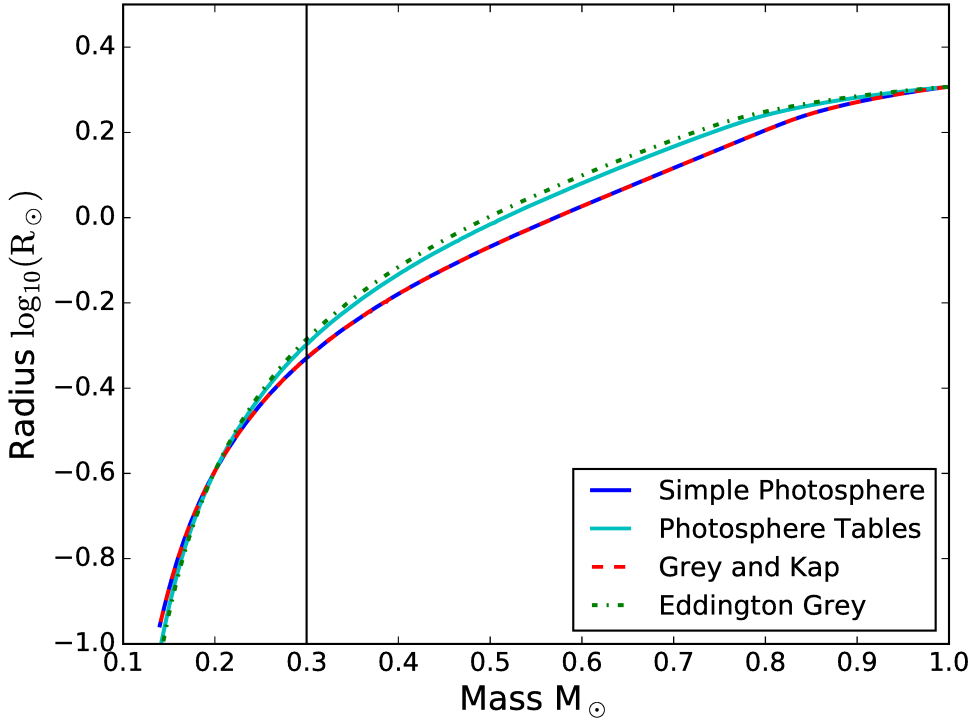


Figure 3.2: The change in radius of the donor star as it is quickly stripped of mass. The vertical black line represents the point where we stop the fast mass loss and place the donor in a binary system.

On the one hand, this surface layer may be capable of losing energy radiatively at the timescale of one year, the same timescale at which we lose mass with `MESA`. Therefore, it may be possible this radiative outer layer is physically motivated. The 3D code used cannot model the loss of energy via radiation and the mass loss rate was an order of magnitude faster than what was used in `MESA`. It may be possible due to the difference in mass loss rates the star was

able to thermally adjust in the case of the MESA model and is not expected to occur in nature. We will not argue if this radiative layer is physically reasonable or not. In both cases however, this outer layer does not dynamically affect the shrinkage of the binary and therefore does not drastically change our results.

3.3 Applications and Results

The grazing encounter formation scenario presented is a possible formation channel of black hole binaries with a semi-degenerate donor. In this case, a low-mass star would have a large portion of its mass stripped in a grazing tidal encounter soon after it has evolved off the main sequence. It is important to note the entire envelope of the donor star is not stripped off, this is the key differentiating factor between this formation scenario and physical collision formation channels considered elsewhere (example. Ivanova et al., 2010). In the work for Ivanova et al. (2017), we looked at a donor star with an initial mass of $1M_{\odot}$ in an eccentric orbit with a $7M_{\odot}$ black hole. The donor star has a metallicity of $Z=0.01$ and is allowed to evolve until it has a radius of $2R_{\odot}$. Once the donor star has reached this radius, it is subjected to a $1M_{\odot} \text{ yr}^{-1}$ mass loss rate to aggressively strip off $0.7M_{\odot}$. It is important to note the mass loss is still not sufficiently high enough to mimic what we would expect in nature. Once the fast mass loss is completed we model the remaining donor star in a binary with the black hole. The binary evolution tracks are shown in Figures 3.3, 3.4 and 3.5. The evolutionary track is also shown in a black dashed line for comparison purposes.

From the results shown in Figures 3.3, 3.4 and 3.5, we see our stripped stars will differ from unperturbed stars with a similar color. We determine how underluminous our stripped star is by taking the difference between the stripped star M_V^{strip} and the unperturbed star M_V^{norm} at the same color $\delta M_V = M_V^{\text{strip}} - M_V^{\text{norm}}$. In the case of the $0.3M_{\odot}$ star in Figure 3.3 at $B-V = 0.8$,

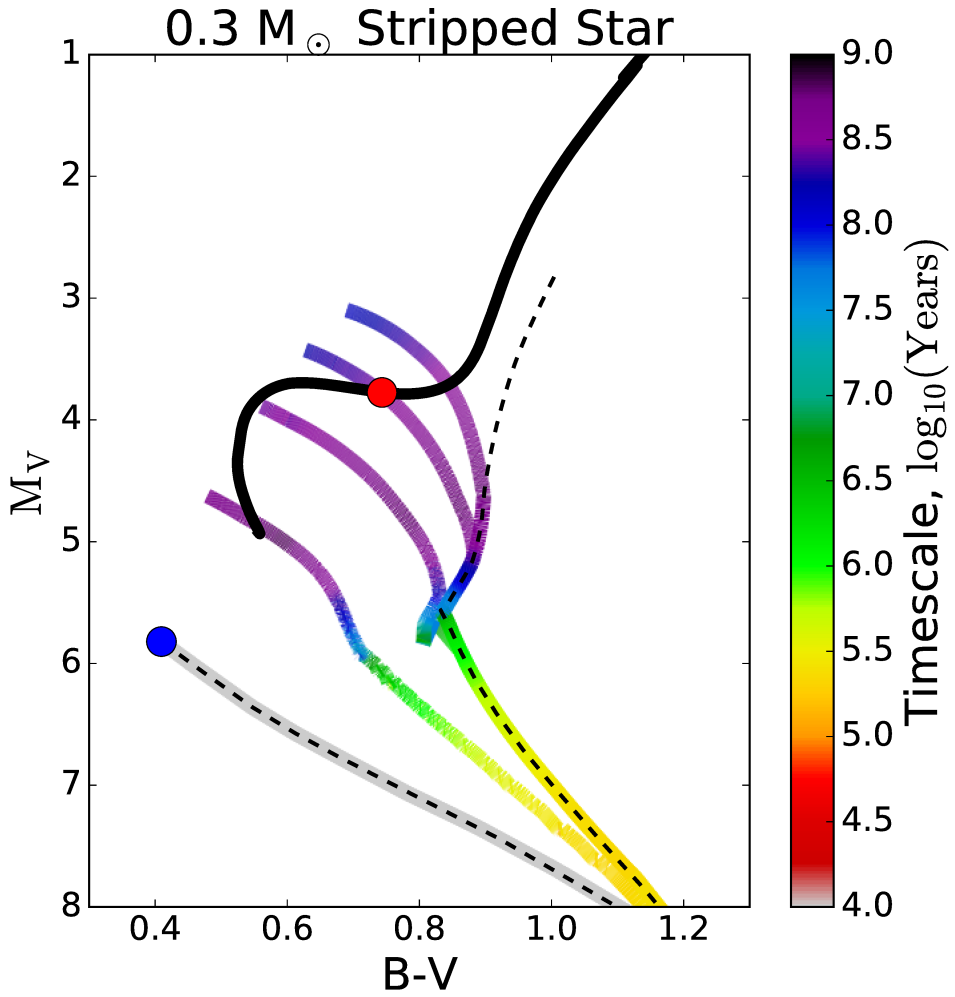


Figure 3.3: A plot comparing the evolution of the $1M_\odot$ star if it remained unperturbed, evolved as a single star after stripping and as a stripped star in a binary system. The black solid line shows the evolutionary track of a $1M_\odot$ star without stripping. The position of the $1M_\odot$ and $2R_\odot$ subgiant prior to the stripping is indicated with the red circle. The location of the stripped star immediately after the stripping down to $0.3M_\odot$ is indicated with the blue circle. The black dashed line shows the evolution of the stripped star as a single star. Tracks with the colors show the evolution of the stripped star in a binary system. The colors of the tracks indicate instantaneous characteristic timescales, such that it takes to change either the magnitude M_V by one or color BV by 0.2. The initial orbital periods are $P_{\text{orb}} = 0.21, 0.54, 0.97$ and 1.46 days.

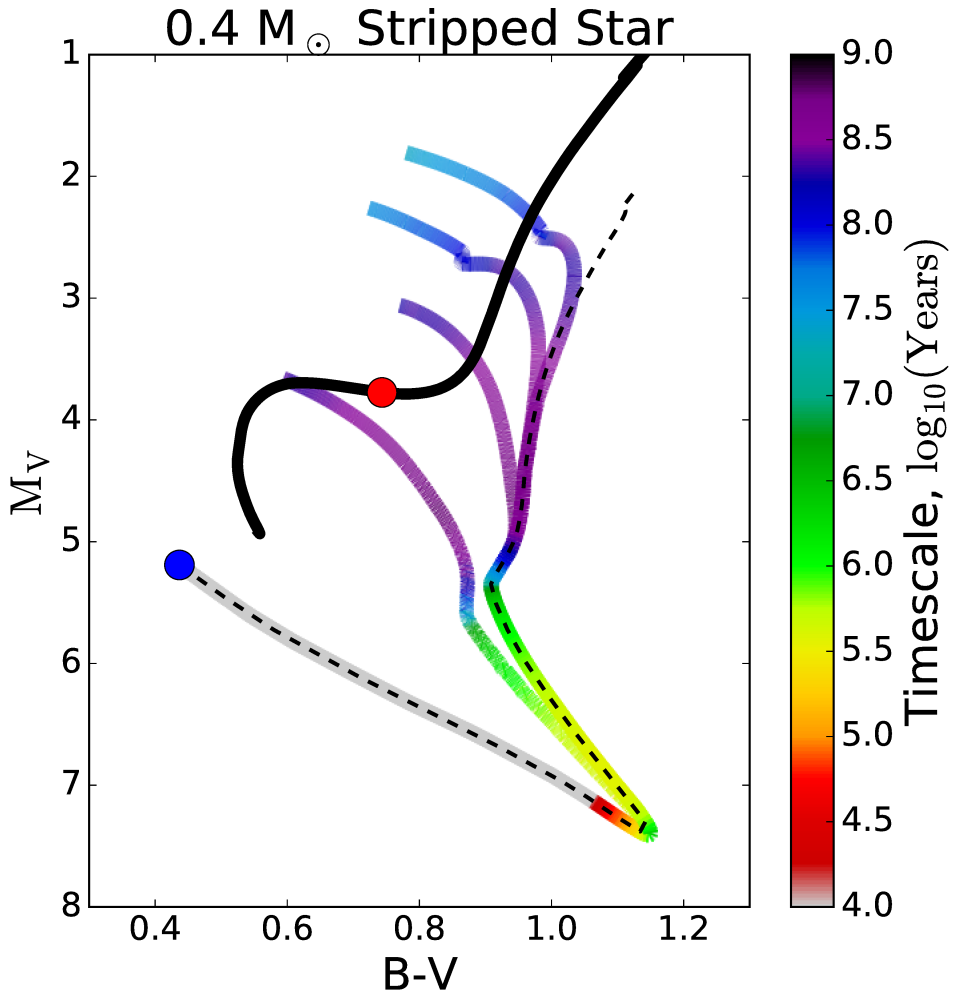


Figure 3.4: The same plot as Figure 3.3 but instead with the case of stripping the donor down to $0.4M_{\odot}$ with initial periods of $P_{\text{orb}} = 0.32, 0.88, 1.62$ and 2.48 days.

the stripped star is underluminous $\delta M_V \gtrsim 2$ for tens of millions of years after stripping and underluminous $2 \gtrsim \delta M_V \gtrsim 1$ for $\sim 3 \times 10^8$ years. Similarly, the $0.4M_{\odot}$ stripped star is underluminous $\delta M_V \gtrsim 1$ for $\sim 1.5 \times 10^8$ years. The $0.5M_{\odot}$ star is also redder than the single star and if we instead compared the stripped star to the unperturbed star at redder colors, it is underluminous $\delta M_V \gtrsim 2$ for $\sim 8 \times 10^8$ years. With this in mind, in cases where a red star is found to be underluminous, $\delta M_V \gtrsim 1$ may be an indicator of this grazing

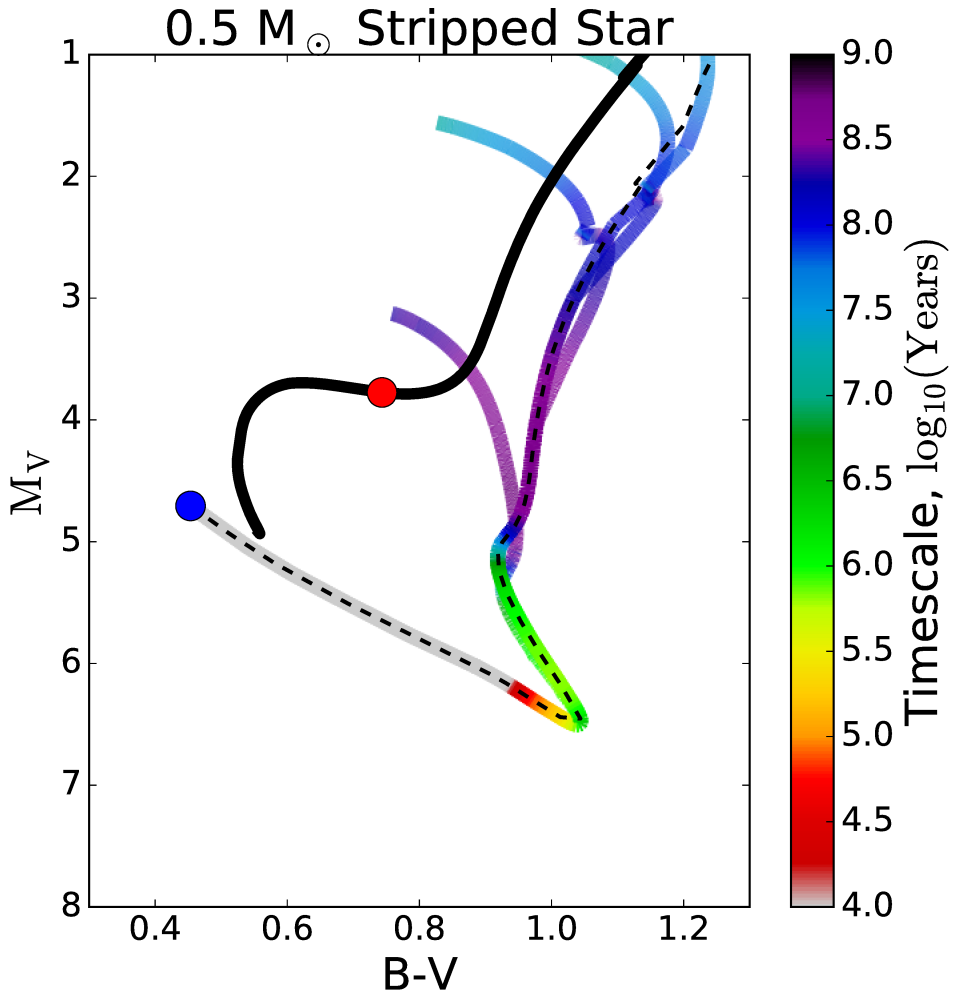


Figure 3.5: The same plot as Figure 3.3 but instead with the case of stripping the donor down to $0.5M_\odot$ with initial periods of $P_{\text{orb}} = 0.42, 1.98, 4.22$ and 6.95 days.

formation. This stripping of the envelope requires a grazing encounter with a compact companion and as such, an underluminous red star may also indicate the existence of a black hole.

Chapter 4

Stability of Mass Transfer in High Mass Donors

4.1 Introduction

With the detection of gravitational wave signals (Abbott et al., 2016a,b, 2017), the understanding and verification of compact object binary mergers is important for constraining possible formation channels. The published detections so far have been for black hole-black hole binaries but as the detectors increase in sensitivity, the possibility of detecting less massive compact objects in these mergers increases (Chen and Amaro-Seoane, 2017). Currently, there are a variety of possible methods in forming binary black holes. Binary black holes can form through dynamic interactions within a globular cluster (Rodriguez et al., 2016) or in isolation. Two dominant channels may form isolated binary black holes: chemically homogeneous evolution (de Mink et al., 2009; Mandel and de Mink, 2016; Marchant et al., 2016) and common envelope evolution (Belczynski et al., 2010).

In the second formation channel, the common envelope event is required to reduce the separation between the two stars. For a common envelope event to occur, the binary must undergo a period of dynamically unstable mass trans-

fer (see Ivanova et al., 2013, for a review on common envelope events). Using standard mass transfer stability criteria, systems with large mass ratios are expected to undergo dynamically unstable mass transfer and result in a common envelope event. Binaries which undergo the a common envelope event may produce a tight black hole black hole binary which will merge in Hubble time. However, if the mass transfer is stable, no common envelope event will occur and should a black hole black hole binary be formed, it will be too wide to merge within Hubble time.

4.2 Stability Criteria

For binary black holes, mass transfer during a massive star’s evolution through the Hertzsprung gap was argued to initiate the runaway mass transfer required for common envelope evolution. Runaway mass transfer normally occurs in binaries where the donor star does not shrink sufficiently quickly while undergoing Roche lobe overflow. As explained in section 1.2.1, the response of the donor is linked to the entropy profile of the star. Stars with large convective envelopes have a flat entropy profile where the response of the donor to mass loss is radial expansion. Should the mass transfer start after the donor has developed a deep convective envelope, the mass transfer will be unstable. Another possibility for rapid expansion during mass loss is if mass transfer occurs as the donor undergoes rapid thermal timescale expansion as a result of its stellar evolution. In Pavlovskii et al. (2017) these points of instability are given as critical radii:

1. Expansion Instability (R_S): This occurs if mass transfer starts as the donor is experiencing thermal timescale expansion. This occurs after the main sequence evolution as the star rapidly expands as it moves onto the Red giant branch. Mass transfer is stable if the donor star has exceeded a radius R_S at the onset of Roche lobe overflow.

2. Convective Instability (R_U): This occurs if mass transfer starts after the donor has developed a deep convective envelope. This results in a flat entropy profile and results in the donor star insufficiently shrinking during mass loss. Mass transfer is stable if it occurs prior to the development of the deep convective zone. This is defined as a critical radius as the star cannot exceed R_U at the onset of Roche lobe overflow.

As mentioned in Section 1.2.1, it is possible for donor stars to start mass transfer in the stability region, $R_S < R < R_U$, but encounter instabilities later in the evolution. It is uncertain if a system will encounter this instability prior to running the simulation.

4.3 Binary Simulations

To calculate the evolution of the binary systems of interest and the stability of mass transfer at Roche lobe overflow, the improved mass transfer prescription described in Section 2.2.1 and Pavlovskii and Ivanova (2015) are used. These models were run using **MESA** version 7736 and **MESA** SDK version 245. The initial donor masses tested were 20, 30, 40, 60 and 80 M_\odot with solar $Z=0.02$ and 0.1 Z_\odot compositions. The donor stars evolve using the “Vink” prescription within **MESA** (Vink et al., 2001). Eruptions and enhanced winds during the luminous blue variable phases are not accounted for. The accretor in each of these binary systems is a black hole with mass between $7M_\odot$ and $14M_\odot$ with a wide range of initial separations tested. It is important to note the evolution of massive stars is very sensitive to the input parameters used. In this work, what is important are the properties of the star at the onset of Roche lobe overflow and it is possible for a range of input conditions to reach this same point.

Table 4.1: Critical Radii For Mass Transfer Stability.

$M_{d,\text{ZAMS}}$	M_{BH}	R_S	$M_{d,S}$	$M_{\text{He},S}$	$H_{\text{sh},S}$	$He_{c,S}$	R_U	$M_{d,U}$	$M_{\text{He},U}$	M_{conv}	$T_{\text{eff},U}$	$H_{\text{sh},U}$	$He_{c,U}$
$Z = 0.1Z_\odot$													
20	7	stable					686-721	19.6	7.0	1.8-3.8	4369-4251	✓	✓
30	7	44-51	29.4	7.7-7.6	✓	—	1004-1111	29.1-29.2	8.1-8.2	1.6*-3.9	4483-4268	✓	✓
40	7	309-354	38.6	11.5	✓	✓	1260-1327	38.6-38.7	11.4	1.7*-2.7	5244-5709	✓	✓
60	7	unstable											
60	10	346-364	56.8	20.4-20.5	✓	—	1705-1790	56.8	19.8	6.0*-6.9*	4473-4387	✓	✓
60	12	140-156	56.8	21.1-20.9	✓	—	1768-1879	56.8	19.8-19.7	6.8*-8.2*	4409-4323	✓	✓
80	7	unstable											
80	10	stable					2217-2241	74.5	32.6	18.2*-18.2*	4285-4276	✓	✓
80	14	134-155	74.6	34.6-34.3	✓	—	2122-2179	74.5	32.7-32.6	18.2*-18.2*	4345-4304	✓	✓
$Z = Z_\odot$													
20	7	stable					729-743	19.6	5.7	2.3-2.7	3936-3886	✓	✓
30	7	stable					1144-1174	26.6	9.8	5.0*-5.5*	3835-3789	✓	—
40	7	stable					1381-1434	32.5	14.7	4.4*-5.2*	3872-3804	✓	—
60	10	stable					2035-2172	41.0	23.8	3.7*-5.0*	3868-3776	✓	—
60	12	stable					2009-2057	41.0	23.8	3.5*-3.9*	3886-3851	✓	—
80	10	stable					stable						
80	14	stable					stable						

Notes. $M_{d,\text{ZAMS}}$ is the mass of the donor at zero age main sequence (ZAMS), M_{BH} is the mass of the accreting black hole. R_S is the radius where the donor star is stable to expansion instability. The lower limit represents the largest radius where expansion instability occurs while the upper limit is the largest radius where the donor can still stably transfer mass. R_U is the radius where the donor star is stable to convective instability. The lower limit represents the largest radius where the donor can stably transfer mass while the upper limit is the smallest radius where the donor has unstable mass transfer. $M_{d,S}$ and $M_{d,U}$ are the masses of the donor at the corresponding radius. $M_{\text{He},S}$ and $M_{\text{He},U}$ are the helium core masses of the donor at the same moment. The boundary of the core is defined as the mass coordinate where hydrogen is below $0.01 \times (1 - Z)$. Check marks under $H_{\text{sh},S}$, $He_{c,S}$, $H_{\text{sh},U}$, and $He_{c,U}$ indicate burning is occurring in the hydrogen shell or helium core. M_{conv} is the mass of the outermost convective layer, an asterisk next to a mass in this column denotes radiative layers exist within the convective zone. $T_{\text{eff},U}$ is the effective temperature at the upper and lower radius values of R_U . If the donor star is always unstable, it is denoted with “unstable”. Stable stars to either type of instability are denoted with “stable” in the appropriate column. All mass values are given in M_\odot , radius in R_\odot , and temperatures in K.

4.4 Results

Table 4.1 (adapted from Pavlovskii et al., 2017) shows the results of the simulations run. The radii given for the two stability boundaries, R_S , and R_U represent the extrema in radius for stability or instability. In the case of R_S the lower limit is the largest unstable value while the upper limit is the smallest stable value. For convective instability R_U this is opposite, the lower limit is the largest stable radius while the upper limit is the smallest unstable radius.

At solar metallicities, if mass transfer occurs after the end of the main sequence the mass transfer is found to be stable. This can be seen in the bottom half of Table 4.1 where all systems with $Z = Z_\odot$ are stable in the R_S column. Systems with sub-solar metallicities vary in stability to the expansion instability. However, in general, systems with lower mass ratio are more stable as can be seen in Table 4.1. The two systems that are always unstable have mass ratios of $q \gtrsim 8.5$ while systems with lower mass ratios show ranges of stability. This is well understood as increasing q results in larger ζ_{RL} . With the criteria for unstable mass transfer being $\zeta_{RL} > \zeta_{ad}$, larger ζ_{RL} values result in systems which are more likely to be unstable (Soberman et al., 1997).

Convective instability appears in systems that have developed a deep convective envelope. Again solar metallicity donors are more stable than the sub-solar systems. This is a result of higher metallicity systems having stronger winds which increase the stability of mass transfer in these systems. An example of this can be seen when comparing the $80M_\odot$ systems in Table 4.1. The solar metallicity systems have strong enough winds suppressing the development of a deep convective envelope and are always stable to this instability, while the sub-solar metallicity case has a range of possible radii. An interesting property of this instability is that many of the systems encounter this instability while there are radiative layers embedded within the convection zone and a single large convective envelope is not necessary.

In Pavlovskii et al. (2017), it was found in the cases where mass transfer begins between these two instabilities, the mass transfer will remain stable. Unless the system reattaches later during its evolution and encounters a delayed dynamical instability, these systems will not undergo a common envelope phase. Without the common envelope evolution, the binary cannot shrink to a radius where a binary black hole merger may occur.

4.4.1 Ultra Luminous X-Ray Sources

With the stable but high mass transfer rates, we can expect the systems to emit large amount of X-ray radiation. Converting mass transfer rate to X-ray luminosity we can use:

$$L_X = \frac{\dot{M}c^2}{2f} \quad (4.1)$$

With L_X being the X-ray luminosity and f representing the inefficiency of the energy being converted from mass. With an inefficiency factor of $f = 1$, the luminosity can approach 10^{39}erg s^{-1} when the mass transfer is a modest $3 \times 10^{-8}M_\odot \text{ yr}^{-1}$. It is important to note the inefficiency factor of $f = 1$ should represent an upper limit and is unlikely for f to reach this value.

Instead of an inefficiency factor, Thorne (1974) used an “efficiency” factor which does not account for the mechanical energy nor advection. This efficiency factor is effectively $\epsilon = \frac{1}{2f}$ and was found to range from ~ 0.06 to ~ 0.42 for a non spinning and maximally spinning black hole respectively. This converts to $f \sim 1.2$ for maximally spinning and $f \sim 8$ for non spinning black holes. To achieve a luminosity of 10^{39}erg s^{-1} a mass transfer rate $\gtrsim 3 \times 10^{-7}M_\odot \text{ yr}^{-1}$ is required for the low efficiency case. For the maximally spinning black hole, a mass transfer rate $\gtrsim 4.2 \times 10^{-8}M_\odot \text{ yr}^{-1}$ is necessary.

In many cases the models tested, can exceed mass transfer rates of $10^{-8}M_\odot \text{ yr}^{-1}$, resulting in very large X-ray luminosities. Systems exceeding a luminosity of

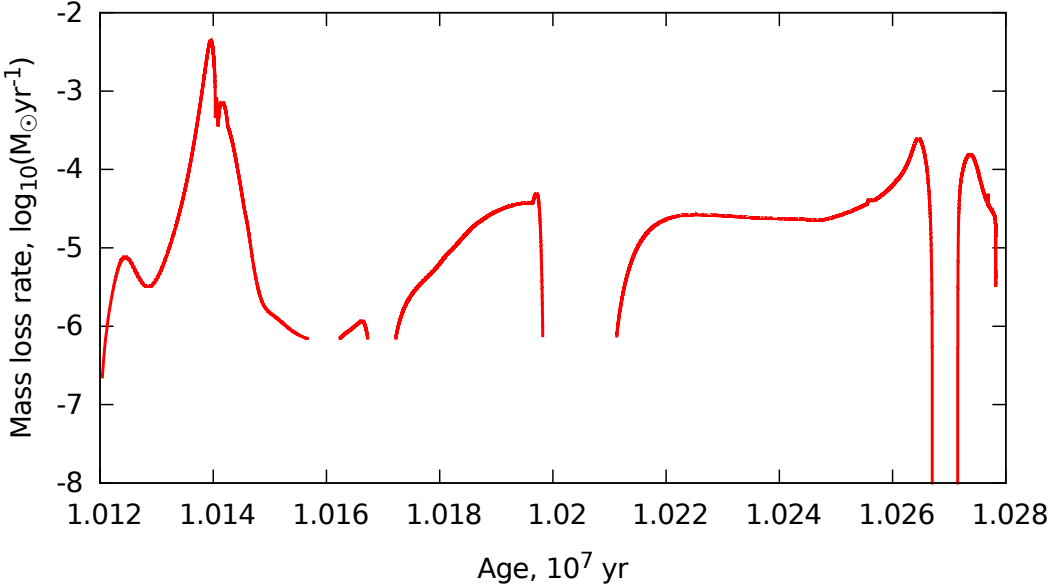


Figure 4.1: A sample of the mass transfer in a binary with a $20 M_{\odot}$ giant and a $7 M_{\odot}$ black hole. The gaps in the evolution track are when the donor detaches. The figure is taken from Pavlovskii et al. (2017).

10^{39} erg s⁻¹ are classified as ultra luminous X-ray (ULX) sources. We can see from Figure 4.1 the mass transfer rates easily exceed those required to reach the ULX threshold luminosity. On the other hand, we also find the models being tested do not spend long periods of time in this ‘‘ULX state’’ of high X-ray luminosity averaging 10^5 yr as the time spent with high luminosity.

4.5 Applications

As a result of an increased parameter space where stable mass transfer may occur, the expected number of merging binary black holes through this formation channel decreases, while the number of ULXs has increased. In the case for ULXs, our models may give a formation channel for the most luminous of ULXs.

Figure 4.2 compares the ULXs found in these simulations against observed ULXs nearby. It is important to note the two separate histograms are averaged

by their respective number of ULXs. With this in mind, our results are not suggesting a large fraction of ULXs are missing from observations with luminosities $> 10^{40}\text{erg s}^{-1}$ but instead, our simulations favour higher luminosity results. To reproduce the entire observed sample of ULX sources, additional formation channels are required to produce the binaries found from 10^{39}erg s^{-1} to 10^{40}erg s^{-1} .

Similarly when applying the new parameter space of stable mass transfer, estimates can be made for the number of black hole merger events we can expect. The LIGO collaboration estimates a stellar-mass binary black hole merger rate in the range of $9 - 240 \text{ Gpc}^{-3}\text{yr}^{-1}$ (Abbott et al., 2016c). Belczynski et al. (2016) found a merger rate of $\gtrsim 1000 \text{ Gpc}^{-3}\text{yr}^{-1}$ prior to accounting for this parameter space with stable mass transfer. A significant fraction of stellar black hole-black hole mergers were initially found to be through this common envelope event channel. With this additional stability range in high mass donors, a drastic decrease in expected binary mergers was found. Using the **STARTRACK** population synthesis code to approximate the effect of this stability range, we can quantify the change in expected binaries. For solar metallicity donors, the number of predicted black hole-black hole binaries produced decreased by a factor of 750, while the sub-solar donors decreased by a factor of 14. Once this stability region is accounted for, the production rate of black hole-black hole mergers decreases to $220 \text{ Gpc}^{-3}\text{yr}^{-1}$, a value within the range found by Abbott et al. (2016c).

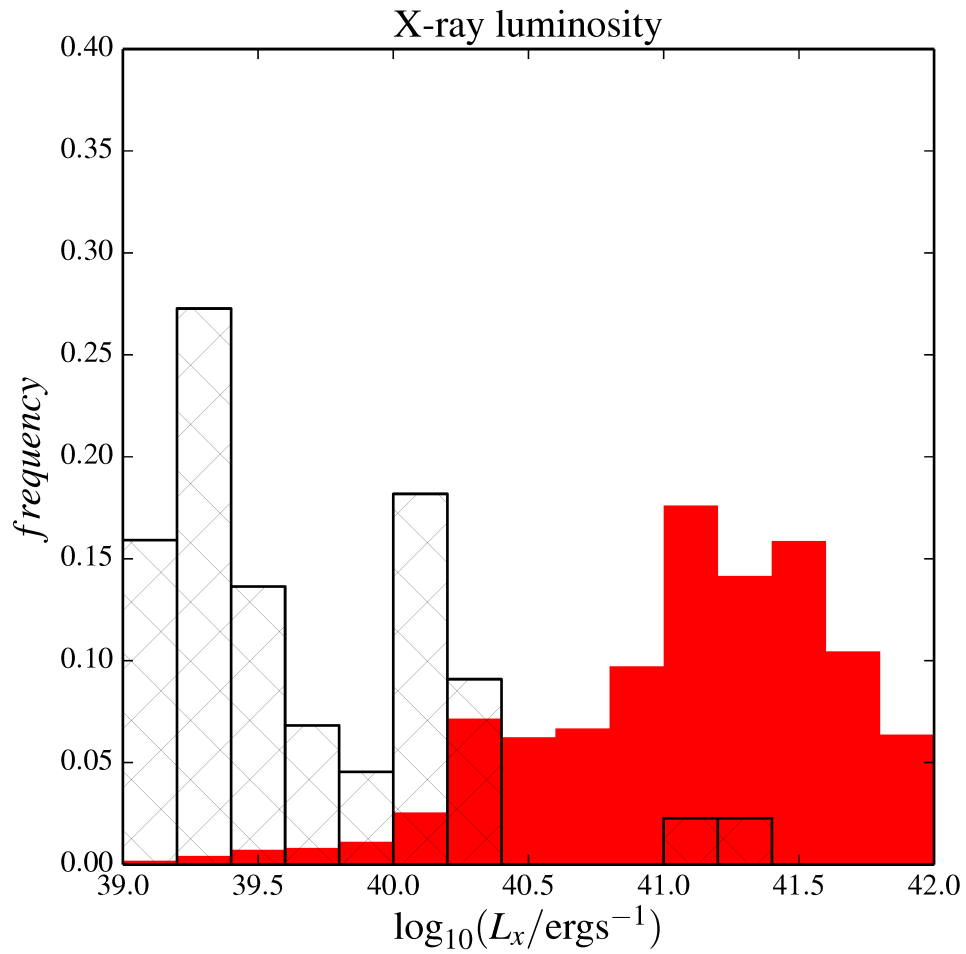


Figure 4.2: A time averaged distribution of ULXs formed in the simulations using conservative mass transfer are given in the red. The observed distributions of ULXs within 5 Mpc are shown in the hatched area (Gladstone et al., 2013). The figure is taken from Pavlovskii et al. (2017).

Chapter 5

Reliability of Current Prescriptions

5.1 Reliability of Roche Lobe Mass Transfer

Within the methods used in this work, there are inherent assumptions made with how various physical processes are treated. **MESA** (Paxton et al., 2011, 2013, 2015) is a one-dimensional stellar evolution code which assumes spherical symmetry and the various stability criteria used only apply in this one-dimensional case. While the assumption of spherical symmetry may be valid in many cases for a star, the outflows of mass from the star are not spherically symmetric and this lack of symmetry may play a role in the mechanics of the outflow. Therefore, the mass transfer rate in **MESA** represents our best understanding of how streamlines which are formed near the L_1 point carry matter.

Beyond the calculation of how mass is transferred, the response of the donor and accretor to the mass transfer is also subject to uncertainties at high mass transfer rates. In the context of this work, the accretor star's only response to mass transfer should be how conservative the process of mass transfer will be. As shown in Section 2.2.2, changes to the Eddington limit result in drastic

changes to the amount of mass lost from the system. With a lower Eddington limit, a smaller amount of mass can be deposited onto the accretor. The difference in mass also affects where the angular momentum of this material is deposited (Priedhorsky and Verbunt, 1988). In the cases where more matter can be accreted onto the compact object, it is possible to spin up the accretor while material lost removes angular momentum from the system.

The largest point of uncertainty is the donor star's response to mass loss. Section 1.2.1 explained depending on the response of the donor star to mass loss, the mass transfer can be dynamically unstable and lead towards a common envelope event or merger event. The mass loss which occurs between thermal and dynamical timescales and the response of the donor to this mass loss is perhaps the most important point in determining the stability. This is the mass loss where proper treatment of the super-adiabatic surface layer has an effect on stability. As explained in Sections 1.2.1 and 1.4.1, the stability of mass transfer at higher values may be overestimated in stars with radiative envelopes and underestimated in stars with convective envelopes. In nature, the outermost portion of the envelope of stars is superadiabatic and transports energy inefficiently through convection. Instead, this outer layer transports energy via both radiative and convective processes. Due to this, the entropy profile of this outermost layer is not flat like the convective envelopes of the star. With this change in entropy profile, the star instead initially contracts as it loses mass.

The outer superadiabatic surface layer of stars can also readjust on timescales shorter than the thermal timescale of the star itself. Therefore, it is possible the surface of the donor star has sufficient time to thermally relax and adjust allowing for the reformation of the superadiabatic layer. As long as the superadiabatic layer can persist, the mass transfer is expected to be more stable (Woods and Ivanova, 2011; Ge et al., 2015).

There are no fully self-consistent prescriptions of mass transfer via Roche

lobe overflow in three-dimensions. However, recent work has been slowly moving towards being able to simulate mass transfer in 3D (Church et al., 2009; Bobrick et al., 2017). With the uncertainties in mind, previous work has shown theoretically calculated values for mass transfer rate are much lower than those found in observations in cases with non-degenerate donors (Podsiadlowski et al., 2002). From the results seen from Podsiadlowski et al. (2002) and Pavlovskii and Ivanova (2016), we see default prescriptions in generating these systems do differ from observed mass transfer rates by an order of magnitude. It is unlikely however, this can be attributed to issues in stability as the observed values for these systems are on order $\sim 10^{-8} - 10^{-7} M_{\odot} \text{ yr}^{-1}$, which is still in the regime where the mass transfer is stable and not large enough to encounter dynamic instability. Looking at observed binaries from Liu et al. (2007), Heinke et al. (2007, 2009, 2013) and Watts and Krishnan (2009), we see the mass transfer rates again are $< 10^{-8} M_{\odot} \text{ yr}^{-1}$ which are too low for dynamically unstable mass transfer rates.

With these uncertainties, systems are expected to result in mass transfer rates lower than observed rates. In cases where the donor star is a non-degenerate donor, the discrepancy between theoretically produced values and observed mass transfer rates is not as great. From Podsiadlowski et al. (2002) and Pavlovskii and Ivanova (2016), the main source of discrepancy is expected to be uncertainties in angular momentum loss. Changing the magnetic braking in Pavlovskii and Ivanova (2016) from default to a boosted prescription resulted in values that better matched observations.

5.2 Reliability of Magnetic Braking

Noted as early as Verbunt and Zwaan (1981), differences in strength of the magnetic field strength results in large changes in the mass transfer rate in binary systems. With the default magnetic braking prescription being calibrated

for single Sun-like stars, it is expected if we deviate too far from these types of systems, the reliability of the default magnetic braking scheme is also expected to decrease (Skumanich, 1972). In general, it has been found the default prescription overestimates the angular momentum lost in quickly rotating systems (van der Sluys et al., 2005). In these cases, a dampening effect is suggested to reduce the strength of the magnetic braking as the strength of the magnetic braking becomes saturated (Mestel and Spruit, 1987; Andronov et al., 2003; Ivanova and Taam, 2003).

On the opposite end of the spectrum, giant stars appear to have their angular momentum loss underestimated by the default magnetic braking and should lose angular momentum more quickly (Smith, 1983). In cases with giant donors, the effects of greater winds and how convective eddies within the star modify the magnetic field strength translate to magnetic braking is not well described with the default prescription (Pavlovskii and Ivanova, 2016).

Reiterating examples of magnetic braking schemes from Section 1.4.3, there are a variety of magnetic braking prescriptions tailored for a variety of different systems.

Examples of this are the prescriptions in Pavlovskii and Ivanova (2016) and Ivanova and Taam (2003). The prescription described in Pavlovskii and Ivanova (2016) is given by equation 1.10 and contains additional scaling with turnover timescales and wind mass loss rates. These additional terms cause the strength of magnetic braking to be reduced in stars with sub-solar winds and convective turnover times and boosted in stars with super-solar values. From Ivanova and Taam (2003), equation 1.12 contains additional scaling based on the rotation rate of the star. Combining the default prescription with these additional scaling terms should, in theory, result in reduced values at shorter periods and boosted values with giant stars compensating for the discrepancies found with the default Skumanich model.

In the work described in Chapters 3 and 4 we used the default Skumanich

model for magnetic braking. One would expect the angular momentum loss may be overestimated for the short period binaries in Chapter 3 and underestimated in the giant donors from Chapter 4.

For the systems tested in Chapter 3, gravitational radiation is becoming the dominant mechanism for angular momentum loss and not magnetic braking. In systems where the binary separation is on the order of a few R_\odot , gravitational radiation becomes dominant. In the case where angular momentum loss is over estimated, the amount of time taken for the onset of mass transfer would increase. Beyond this, the amount of time spent in each portion of the color magnitude diagram would likely not differ greatly as the mass transfer rate in these areas is already low.

In Chapter 4, the stability criteria depends on the point in evolution where mass transfer starts. If mass transfer occurs within the stability region, then we expect mass transfer to remain stable regardless of magnetic braking prescription. As such, our choice of magnetic braking does not affect our final result in determining regions of stable mass transfer.

While the work described above is not greatly affected by choices in magnetic braking, studies involving long lived steady state mass transfer are. Changes in the γ_{mb} value result in large changes in the binary evolution (Rappaport et al., 1983). While $\gamma_{mb} = 4$ is commonly used as it reproduces the spin down of G type main sequence stars, other γ_{mb} values have been used. $\gamma_{mb} = 3$ has been used by Knigge et al. (2011) to produce cataclysmic variables while $\gamma_{mb} = 5$ was recently applied by Istrate et al. (2014) to form ultra-compact systems. A “best” choice in γ_{mb} may be difficult to determine prior to testing a variety of γ_{mb} values. Beyond these uncertainties with the used prescription of magnetic braking, it is possible prescriptions created for similar systems may result in drastically different results (Knigge et al., 2011).

Uncertainties in the stability of mass transfer rate results in systems of high mass transfer incorrectly predicted to be unstable. This results in un-

derestimating the number of high mass transfer systems in simulations when compared to observations. Another possible source of this discrepancy is likely a lack of understanding behind the mechanics of magnetic braking. Instead, the uncertainties in mass transfer rate relate to the stability of the mass transfer and will likely play a role in higher mass transfer rates. Improvements to the response of the donor star as mass transfer occurs will affect the properties of the binary but without testing the models with these changes to donor response, it is uncertain how these binaries would differ. The uncertainties from magnetic braking prescriptions have overarching effects on the results of models. Magnetic braking models are created and calibrated to subsets of systems and cannot be applied to the entirety of a binary system's evolution. A more complete prescription of magnetic braking is required in order to make definitive claims about theoretical models.

Chapter 6

Summary and Conclusions

In this thesis, we explored a variety of topics related to binary evolution ranging from how interactions prior to mass transfer can drastically change the outcome of the system in Chapter 3 to the stability of mass transfer in Chapter 4.

We find in cases where a binary is dynamically formed through a grazing tidal encounter, a process that strips off a large portion of the outer envelope, the resulting binary differs greatly from an unperturbed star. In the case where the star has undergone this grazing tidal encounter, the resulting semi-degenerate donor may be underluminous by up to two orders of magnitude for several million years depending on the amount of mass lost. A caveat of this result however, is the stellar evolution code used, `MESA`, is not designed for the high mass loss rates required to strip the envelope. As a result of this, we could not remove the envelope at a rate higher than $1M_{\odot}\text{yr}^{-1}$. In addition to the lower than ideal mass loss rate is the formation of a low mass radiative surface layer in the semi-degenerate donors. It was found in 3D simulations the resulting semi-degenerate star would be $0.32R_{\odot}$ while the thin radiative envelope on our donors result in a larger $0.47R_{\odot}$ radius. It is unknown if this outer radiative layer is physically motivated as the 3D code does not model energy loss through radiation while the 1D code cannot reach the required mass transfer rates. Regardless of this, the outer layer does not affect the shrinkage

of the binary and as such, does not drastically change our result. Therefore, we propose an underluminous red star may indicate the star underwent a grazing tidal encounter.

In Chapter 4, we looked at the stability of mass transfer in binaries with a high mass donor. Recently, with the detection of gravitational waves (Abbott et al., 2016a,b, 2017), constraining and understanding the formation of systems which can produce possible compact object mergers has become an important topic of research. One of the key formation channels to produce compact binary mergers involves a common envelope event and as such, requires unstable mass transfer. We found the stability of mass transfer in these systems relied heavily on mass transfer occurring between two points of instability:

1. Expansion Instability (R_S): The point in evolution where the star undergoes rapid expansion after leaving the main sequence.
2. Convective Instability (R_U): The point in evolution where the star has developed a deep convective envelope. Stars with a deep convective envelope do not shrink a sufficient amount during mass loss.

If the mass transfer occurs between these two points, $R_S < R_d < R_U$ then mass transfer is initially stable. Applying the improved mass transfer prescription from Pavlovskii and Ivanova (2015), we found many systems experience stable mass transfer despite having very large mass ratios. If mass transfer is stable in these systems, it is unlikely they will result in a gravitational wave signal as the two compact objects are not close enough without undergoing the common envelope phase. Instead, a portion of these systems which were initially thought to result in gravitational wave signals will instead result in X-ray binaries. With such high mass transfer rates, the resulting X-ray luminosity of these systems is $10^{40} \text{ erg s}^{-1}$ which places our systems in the range of ultra luminous X-ray sources.

Bibliography

- B. P. Abbott, R. Abbott, T. D. Abbott, M. R. Abernathy, F. Acernese, K. Ackley, C. Adams, T. Adams, P. Addesso, R. X. Adhikari, and et al. Observation of Gravitational Waves from a Binary Black Hole Merger. *Physical Review Letters*, 116(6):061102, February 2016a. doi: 10.1103/PhysRevLett.116.061102.
- B. P. Abbott, R. Abbott, T. D. Abbott, M. R. Abernathy, F. Acernese, K. Ackley, C. Adams, T. Adams, P. Addesso, R. X. Adhikari, and et al. GW151226: Observation of Gravitational Waves from a 22-Solar-Mass Binary Black Hole Coalescence. *Physical Review Letters*, 116(24):241103, June 2016b. doi: 10.1103/PhysRevLett.116.241103.
- B. P. Abbott, R. Abbott, T. D. Abbott, M. R. Abernathy, F. Acernese, K. Ackley, C. Adams, T. Adams, P. Addesso, R. X. Adhikari, and et al. Binary Black Hole Mergers in the First Advanced LIGO Observing Run. *Physical Review X*, 6(4):041015, October 2016c. doi: 10.1103/PhysRevX.6.041015.
- B. P. Abbott, R. Abbott, T. D. Abbott, F. Acernese, K. Ackley, C. Adams, T. Adams, P. Addesso, R. X. Adhikari, V. B. Adya, and et al. GW170104: Observation of a 50-Solar-Mass Binary Black Hole Coalescence at Redshift 0.2. *Physical Review Letters*, 118(22):221101, June 2017. doi: 10.1103/PhysRevLett.118.221101.

- H. A. Abt and S. G. Levy. Multiplicity among solar-type stars. *ApJS*, 30: 273–306, March 1976. doi: 10.1086/190363.
- N. Andronov, M. Pinsonneault, and A. Sills. Cataclysmic Variables: An Empirical Angular Momentum Loss Prescription from Open Cluster Data. *ApJ*, 582:358–368, January 2003. doi: 10.1086/343030.
- D. Bacon, S. Sigurdsson, and M. B. Davies. Close approach during hard binary-binary scattering. *MNRAS*, 281:830–846, August 1996. doi: 10.1093/mnras/281.3.830.
- C. D. Bailyn. Blue Stragglers and Other Stellar Anomalies: Implications for the Dynamics of Globular Clusters. *ARA&A*, 33:133–162, 1995. doi: 10.1146/annurev.aa.33.090195.001025.
- K. Belczynski, M. Dominik, T. Bulik, R. O’Shaughnessy, C. Fryer, and D. E. Holz. The Effect of Metallicity on the Detection Prospects for Gravitational Waves. *ApJ*, 715:L138–L141, June 2010. doi: 10.1088/2041-8205/715/2/L138.
- K. Belczynski, S. Repetto, D. E. Holz, R. O’Shaughnessy, T. Bulik, E. Berti, C. Fryer, and M. Dominik. Compact Binary Merger Rates: Comparison with LIGO/Virgo Upper Limits. *ApJ*, 819:108, March 2016. doi: 10.3847/0004-637X/819/2/108.
- A. Bobrick, M. B. Davies, and R. P. Church. Mass transfer in white dwarf-neutron star binaries. *MNRAS*, 467:3556–3575, May 2017. doi: 10.1093/mnras/stx312.
- M. G. Bowler. Interpretation of observations of the circumbinary disk of SS 433. *A&A*, 521:A81, October 2010. doi: 10.1051/0004-6361/201014711.
- B. W. Carroll and D. A. Ostlie. An introduction to modern astrophysics and cosmology. July 2006.

- W.-C. Chen and P. Podsiadlowski. Evolution of Intermediate-mass X-Ray Binaries Driven by the Magnetic Braking of AP/BP Stars. I. Ultracompact X-Ray Binaries. *ApJ*, 830:131, October 2016. doi: 10.3847/0004-637X/830/2/131.
- X. Chen and P. Amaro-Seoane. Revealing the formation of stellar-mass black hole binaries: The need for deci-Hertz gravitational wave observatories. *ArXiv e-prints*, February 2017.
- R. P. Church, J. Dischler, M. B. Davies, C. A. Tout, T. Adams, and M. E. Beer. Mass transfer in eccentric binaries: the new oil-on-water smoothed particle hydrodynamics technique. *MNRAS*, 395:1127–1134, May 2009. doi: 10.1111/j.1365-2966.2009.14619.x.
- E. J. M. Colbert and R. F. Mushotzky. The Nature of Accreting Black Holes in Nearby Galaxy Nuclei. *ApJ*, 519:89–107, July 1999. doi: 10.1086/307356.
- M. Coriat, R. P. Fender, and G. Dubus. Revisiting a fundamental test of the disc instability model for X-ray binaries. *MNRAS*, 424:1991–2001, August 2012. doi: 10.1111/j.1365-2966.2012.21339.x.
- S. E. de Mink, M. Cantiello, N. Langer, O. R. Pols, I. Brott, and S.-C. Yoon. Rotational mixing in massive binaries. Detached short-period systems. *A&A*, 497:243–253, April 2009. doi: 10.1051/0004-6361/200811439.
- G. Duchêne and A. Kraus. Stellar Multiplicity. *ARA&A*, 51:269–310, August 2013. doi: 10.1146/annurev-astro-081710-102602.
- A. S. Eddington. *The Internal Constitution of the Stars*. 1926.
- P. Eggleton. *Evolutionary Processes in Binary and Multiple Stars*. July 2006.
- P. P. Eggleton. Approximations to the radii of Roche lobes. *ApJ*, 268:368, May 1983. doi: 10.1086/160960.

- A. C. Fabian, J. E. Pringle, and M. J. Rees. Tidal capture formation of binary systems and X-ray sources in globular clusters. *MNRAS*, 172:15p–18p, August 1975. doi: 10.1093/mnras/172.1.15P.
- E. Gaburov, J. C. Lombardi, Jr., and S. Portegies Zwart. On the onset of runaway stellar collisions in dense star clusters - II. Hydrodynamics of three-body interactions. *MNRAS*, 402:105–126, February 2010. doi: 10.1111/j.1365-2966.2009.15900.x.
- H. Ge, M. S. Hjellming, R. F. Webbink, X. Chen, and Z. Han. Adiabatic Mass Loss in Binary Stars. I. Computational Method. *ApJ*, 717:724–738, July 2010. doi: 10.1088/0004-637X/717/2/724.
- H. Ge, R. F. Webbink, X. Chen, and Z. Han. Adiabatic Mass Loss in Binary Stars. II. From Zero-age Main Sequence to the Base of the Giant Branch. *ApJ*, 812:40, October 2015. doi: 10.1088/0004-637X/812/1/40.
- J. C. Gladstone, C. Copperwheat, C. O. Heinke, T. P. Roberts, T. F. Cartwright, A. J. Levan, and M. R. Goad. Optical Counterparts of the Nearest Ultraluminous X-Ray Sources. *ApJS*, 206:14, June 2013. doi: 10.1088/0067-0049/206/2/14.
- C. O. Heinke, P. G. Jonker, R. Wijnands, and R. E. Taam. Constraints on Thermal X-Ray Radiation from SAX J1808.4-3658 and Implications for Neutron Star Neutrino Emission. *ApJ*, 660:1424–1427, May 2007. doi: 10.1086/513140.
- C. O. Heinke, P. G. Jonker, R. Wijnands, C. J. Deloye, and R. E. Taam. Further Constraints on Thermal Quiescent X-Ray Emission from SAX J1808.4-3658. *ApJ*, 691:1035–1041, February 2009. doi: 10.1088/0004-637X/691/2/1035.
- C. O. Heinke, N. Ivanova, M. C. Engel, K. Pavlovskii, G. R. Sivakoff, T. F. Cartwright, and J. C. Gladstone. Galactic Ultracompact X-Ray Binaries:

Disk Stability and Evolution. *ApJ*, 768:184, May 2013. doi: 10.1088/0004-637X/768/2/184.

W. Herschel. Catalogue of 500 New Nebulae, Nebulous Stars, Planetary Nebulae, and Clusters of Stars; With Remarks on the Construction of the Heavens. *Philosophical Transactions of the Royal Society of London Series I*, 92:477–528, 1802.

S. Hinata. An approximate analytic solution of a set of nonlinear model alpha-omega-dynamo equations for marginally unstable systems. *Ap&SS*, 153:1–11, March 1989. doi: 10.1007/BF00643605.

M. S. Hjellming and R. F. Webbink. Thresholds for rapid mass transfer in binary systems. I - Polytropic models. *ApJ*, 318:794–808, July 1987. doi: 10.1086/165412.

A. G. Istrate, T. M. Tauris, and N. Langer. The formation of low-mass helium white dwarfs orbiting pulsars . Evolution of low-mass X-ray binaries below the bifurcation period. *A&A*, 571:A45, November 2014. doi: 10.1051/0004-6361/201424680.

N. Ivanova. Low-Mass X-Ray Binaries with Pre-Main-Sequence Companions. *ApJ*, 653:L137–L140, December 2006. doi: 10.1086/510672.

N. Ivanova and J. L. A. Nandez. Common envelope events with low-mass giants: understanding the transition to the slow spiral-in. *MNRAS*, 462: 362–381, October 2016. doi: 10.1093/mnras/stw1676.

N. Ivanova and R. E. Taam. Magnetic Braking Revisited. *ApJ*, 599:516–521, December 2003. doi: 10.1086/379192.

N. Ivanova, S. Chaichenets, J. Fregeau, C. O. Heinke, J. C. Lombardi, Jr., and T. E. Woods. Formation of Black Hole X-ray Binaries in Globular Clusters. *ApJ*, 717:948–957, July 2010. doi: 10.1088/0004-637X/717/2/948.

- N. Ivanova, S. Justham, X. Chen, O. De Marco, C. L. Fryer, E. Gaburov, H. Ge, E. Glebbeek, Z. Han, X.-D. Li, G. Lu, T. Marsh, P. Podsiadlowski, A. Potter, N. Soker, R. Taam, T. M. Tauris, E. P. J. van den Heuvel, and R. F. Webbink. Common envelope evolution: where we stand and how we can move forward. *A&ARv*, 21:59, February 2013. doi: 10.1007/s00159-013-0059-2.
- N. Ivanova, C. A. da Rocha, K. X. Van, and J. L. A. Nandez. Formation of black hole X-ray binaries with non-degenerate donors in globular clusters. *ArXiv e-prints*, June 2017.
- S. Justham, S. Rappaport, and P. Podsiadlowski. Magnetic braking of Ap/Bp stars: application to compact black-hole X-ray binaries. *MNRAS*, 366:1415–1423, March 2006. doi: 10.1111/j.1365-2966.2005.09907.x.
- C. Knigge, I. Baraffe, and J. Patterson. The Evolution of Cataclysmic Variables as Revealed by Their Donor Stars. *ApJS*, 194:28, June 2011. doi: 10.1088/0067-0049/194/2/28.
- H. A. Kobulnicky, R. A. Smullen, D. C. Kiminki, J. C. Runnoe, E. S. Wood, G. Long, M. J. Alexander, M. J. Lundquist, and C. Vargas-Alvarez. A Fresh Catch of Massive Binaries in the Cygnus OB2 Association. *ApJ*, 756:50, September 2012. doi: 10.1088/0004-637X/756/1/50.
- H. A. Kobulnicky, D. C. Kiminki, M. J. Lundquist, J. Burke, J. Chapman, E. Keller, K. Lester, E. K. Rolen, E. Topel, A. Bhattacharjee, R. A. Smullen, C. A. Vargas Álvarez, J. C. Runnoe, D. A. Dale, and M. M. Brotherton. Toward Complete Statistics of Massive Binary Stars: Penultimate Results from the Cygnus OB2 Radial Velocity Survey. *ApJS*, 213:34, August 2014. doi: 10.1088/0067-0049/213/2/34.
- Z. Kopal. The classification of close binary systems. *Annales d’Astrophysique*, 18:379, January 1955.

- R. P. Kraft, J. Mathews, and J. L. Greenstein. Binary Stars among Cataclysmic Variables. II. Nova WZ Sagittae: a Possible Radiator of Gravitational Waves. *ApJ*, 136:312–315, July 1962. doi: 10.1086/147381.
- L. D. Landau and E. M. Lifshitz. *The classical theory of fields*. 1975.
- J.-P. Lasota. The disc instability model of dwarf novae and low-mass X-ray binary transients. *New Astron. Rev.*, 45:449–508, June 2001. doi: 10.1016/S1387-6473(01)00112-9.
- J.-P. Lasota. Physics of accretion flows around compact objects. *Comptes Rendus Physique*, 8:45–56, January 2007. doi: 10.1016/j.crhy.2006.11.002.
- J.-P. Lasota. Black Hole Accretion Discs. *Astrophysics of Black Holes: From Fundamental Aspects to Latest Developments*, 440:1, 2016. doi: 10.1007/978-3-662-52859-4_1.
- Q. Z. Liu, J. van Paradijs, and E. P. J. van den Heuvel. A catalogue of low-mass X-ray binaries in the Galaxy, LMC, and SMC (Fourth edition). *A&A*, 469: 807–810, July 2007. doi: 10.1051/0004-6361:20077303.
- J. C. Lombardi, Jr., W. Holtzman, K. L. Dooley, K. Gearity, V. Kalogera, and F. A. Rasio. Twin Binaries: Studies of Stability, Mass Transfer, and Coalescence. *ApJ*, 737:49, August 2011. doi: 10.1088/0004-637X/737/2/49.
- I. Mandel and S. E. de Mink. Merging binary black holes formed through chemically homogeneous evolution in short-period stellar binaries. *MNRAS*, 458:2634–2647, May 2016. doi: 10.1093/mnras/stw379.
- P. Marchant, N. Langer, P. Podsiadlowski, T. M. Tauris, and T. J. Moriya. A new route towards merging massive black holes. *A&A*, 588:A50, April 2016. doi: 10.1051/0004-6361/201628133.
- B. D. Mason, D. R. Gies, W. I. Hartkopf, W. G. Bagnuolo, Jr., T. ten Brummelaar, and H. A. McAlister. ICCD speckle observations of binary stars.

- XIX - an astrometric/spectroscopic survey of O stars. *AJ*, 115:821, February 1998. doi: 10.1086/300234.
- L. Mestel and H. C. Spruit. On magnetic braking of late-type stars. *MNRAS*, 226:57–66, May 1987. doi: 10.1093/mnras/226.1.57.
- N. Meunier, M. R. E. Proctor, D. D. Sokoloff, A. M. Soward, and S. M. Tobias. Asymptotic properties of a nonlinéar -dynamo wave: Period, amplitude and latitude dependence. *Geophysical and Astrophysical Fluid Dynamics*, 86: 249–285, 1997. doi: 10.1080/03091929708245464.
- F. Meyer and E. Meyer-Hofmeister. On the Elusive Cause of Cataclysmic Variable Outbursts. *A&A*, 104:L10, 1981.
- J. Michell. An Inquiry into the Probable Parallax, and Magnitude of the Fixed Stars, from the Quantity of Light Which They Afford us, and the Particular Circumstances of Their Situation, by the Rev. John Michell, B. D. F. R. S. *Philosophical Transactions of the Royal Society of London Series I*, 57: 234–264, 1767.
- S. W. Mochnacki. Accurate integrations of the Roche model. *ApJS*, 55:551–561, August 1984. doi: 10.1086/190967.
- J. L. A. Nandez, N. Ivanova, and J. C. Lombardi, Jr. V1309 Sco-Understanding a Merger. *ApJ*, 786:39, May 2014. doi: 10.1088/0004-637X/786/1/39.
- R. W. Noyes, L. W. Hartmann, S. L. Baliunas, D. K. Duncan, and A. H. Vaughan. Rotation, convection, and magnetic activity in lower main-sequence stars. *ApJ*, 279:763–777, April 1984. doi: 10.1086/161945.
- B. Paczynski. Common Envelope Binaries. In P. Eggleton, S. Mitton, and J. Whelan, editors, *Structure and Evolution of Close Binary Systems*, volume 73 of *IAU Symposium*, page 75, 1976.

- E. N. Parker. The Generation of Magnetic Fields in Astrophysical Bodies.IV. The Solar and Terrestrial Dynamos. *ApJ*, 164:491, March 1971. doi: 10.1086/150862.
- K. Pavlovskii and N. Ivanova. Mass transfer from giant donors. *MNRAS*, 449: 4415–4427, June 2015. doi: 10.1093/mnras/stv619.
- K. Pavlovskii and N. Ivanova. Mass transfer and magnetic braking in Sco X-1. *MNRAS*, 456:263–269, February 2016. doi: 10.1093/mnras/stv2685.
- K. Pavlovskii, N. Ivanova, K. Belczynski, and K. X. Van. Stability of mass transfer from massive giants: double black hole binary formation and ultraluminous X-ray sources. *MNRAS*, 465:2092–2100, February 2017. doi: 10.1093/mnras/stw2786.
- B. Paxton, L. Bildsten, A. Dotter, F. Herwig, P. Lesaffre, and F. Timmes. Modules for Experiments in Stellar Astrophysics (MESA). *ApJS*, 192:3, January 2011. doi: 10.1088/0067-0049/192/1/3.
- B. Paxton, M. Cantiello, P. Arras, L. Bildsten, E. F. Brown, A. Dotter, C. Mankovich, M. H. Montgomery, D. Stello, F. X. Timmes, and R. Townsend. Modules for Experiments in Stellar Astrophysics (MESA): Planets, Oscillations, Rotation, and Massive Stars. *ApJS*, 208:4, September 2013. doi: 10.1088/0067-0049/208/1/4.
- B. Paxton, P. Marchant, J. Schwab, E. B. Bauer, L. Bildsten, M. Cantiello, L. Dessart, R. Farmer, H. Hu, N. Langer, R. H. D. Townsend, D. M. Townsley, and F. X. Timmes. Modules for Experiments in Stellar Astrophysics (MESA): Binaries, Pulsations, and Explosions. *ApJS*, 220:15, September 2015. doi: 10.1088/0067-0049/220/1/15.
- S. Perez M. and K. M. Blundell. SS433’s circumbinary ring and accretion disc

viewed through its attenuating disc wind. *MNRAS*, 408:2–8, October 2010.
doi: 10.1111/j.1365-2966.2010.16638.x.

P. Podsiadlowski, S. Rappaport, and E. D. Pfahl. Evolutionary Sequences for Low- and Intermediate-Mass X-Ray Binaries. *ApJ*, 565:1107–1133, February 2002. doi: 10.1086/324686.

W. C. Priedhorsky and F. Verbunt. Tidal forces and mass transfer instabilities in low-mass X-ray binaries. *ApJ*, 333:895–905, October 1988. doi: 10.1086/166798.

S. Rappaport, F. Verbunt, and P. C. Joss. A new technique for calculations of binary stellar evolution, with application to magnetic braking. *ApJ*, 275: 713–731, December 1983. doi: 10.1086/161569.

M. Renzo, C. D. Ott, S. N. Shore, and S. E. de Mink. A Systematic Survey of the Effects of Wind Mass Loss Algorithms on the Evolution of Single Massive Stars. *ArXiv e-prints*, March 2017.

H. Ritter. Turning on and off mass transfer in cataclysmic binaries. *A&A*, 202: 93–100, August 1988.

C. L. Rodriguez, S. Chatterjee, and F. A. Rasio. Binary black hole mergers from globular clusters: Masses, merger rates, and the impact of stellar evolution. *Phys. Rev. D*, 93(8):084029, April 2016. doi: 10.1103/PhysRevD.93.084029.

H. Sana, S. E. de Mink, A. de Koter, N. Langer, C. J. Evans, M. Gieles, E. Gosset, R. G. Izzard, J.-B. Le Bouquin, and F. R. N. Schneider. Binary Interaction Dominates the Evolution of Massive Stars. *Science*, 337:444, July 2012. doi: 10.1126/science.1223344.

R. Sengar, T. M. Tauris, N. Langer, and A. G. Istrate. Novel modelling of ultra-compact X-ray binary evolution - stable mass transfer from white dwarfs to neutron stars. *ArXiv e-prints*, April 2017.

- J. F. Sepinsky, B. Willems, V. Kalogera, and F. A. Rasio. Interacting Binaries with Eccentric Orbits: Secular Orbital Evolution Due to Conservative Mass Transfer. *ApJ*, 667:1170–1184, October 2007. doi: 10.1086/520911.
- A. Skumanich. Time Scales for CA II Emission Decay, Rotational Braking, and Lithium Depletion. *ApJ*, 171:565, February 1972. doi: 10.1086/151310.
- R. C. Smith. Stellar rotation: Magnetic brakes on giant stars. *Nature*, 303: 130–131, May 1983. doi: 10.1038/303130a0.
- G. E. Soberman, E. S. Phinney, and E. P. J. van den Heuvel. Stability criteria for mass transfer in binary stellar evolution. *A&A*, 327:620–635, November 1997.
- T. M. Tauris and E. P. J. van den Heuvel. *Formation and evolution of compact stellar X-ray sources*, pages 623–665. April 2006.
- K. S. Thorne. Disk-Accretion onto a Black Hole. II. Evolution of the Hole. *ApJ*, 191:507–520, July 1974. doi: 10.1086/152991.
- M. V. van der Sluys, F. Verbunt, and O. R. Pols. Reduced magnetic braking and the magnetic capture model for the formation of ultra-compact binaries. *A&A*, 440:973–979, September 2005. doi: 10.1051/0004-6361:20052696.
- F. Verbunt and C. Zwaan. Magnetic braking in low-mass X-ray binaries. *A&A*, 100:L7–L9, July 1981.
- J. S. Vink, A. de Koter, and H. J. G. L. M. Lamers. Mass-loss predictions for O and B stars as a function of metallicity. *A&A*, 369:574–588, April 2001. doi: 10.1051/0004-6361:20010127.
- A. L. Watts and B. Krishnan. Detecting gravitational waves from accreting neutron stars. *Advances in Space Research*, 43:1049–1054, April 2009. doi: 10.1016/j.asr.2009.01.006.

- R. F. Webbink. *Stellar evolution and binaries*, page 39. 1985.
- J. M. Weisberg and J. H. Taylor. The Relativistic Binary Pulsar B1913+16: Thirty Years of Observations and Analysis. In F. A. Rasio and I. H. Stairs, editors, *Binary Radio Pulsars*, volume 328 of *Astronomical Society of the Pacific Conference Series*, page 25, July 2005.
- T. E. Woods and N. Ivanova. Can We Trust Models for Adiabatic Mass Loss? *ApJ*, 739:L48, October 2011. doi: 10.1088/2041-8205/739/2/L48.
- J.-P. Zahn and L. Bouchet. Tidal evolution of close binary stars. II - Orbital circularization of late-type binaries. *A&A*, 223:112–118, October 1989.

Appendix A

Custom MESA Routines

In this section I include the code used to modify or extend the capabilities of `MESA`. To use these additions the user must copy the respective subroutine into `run_binary_extras.f` and point to the subroutine in the code. These changes were applied to `MESA` 8677 and in principle should be applicable to other version of `MESA` as well, with the quick revision cycles with `MESA` updates variable names may change from one version to another.

A.1 Implementation of Eddington Limit

```
subroutine mdot_edd_routine(binary_id, mdot_edd, ierr)
    use const_def, only: dp
    integer, intent(in) :: binary_id
    real(dp), intent(out) :: mdot_edd
    integer, intent(out) :: ierr
    type (binary_info), pointer :: b
    ierr = 0
    call binary_ptr(binary_id, b, ierr)
    if (ierr /= 0) then
        write(*,*) 'failed in binary_ptr'
```

```

        return
    end if

    ! changing mdot_edd from default MESA from BH to NS
    ! x_ctrl(5) is the radius of the NS

    ! mdot_edd = 4*pi*cight*b% s1% x_ctrl(5)/&
    !           (0.2*(1+b% s1% surface_h1))
    ! hard coding in the radius of 11.5km into the
    ! equation results in the next line.
    mdot_edd = 2.1666d18 / (1.d0 + b% s1% surface_h1)
end subroutine mdot_edd_routine

```

A.2 Implementation of Magnetic Braking

```

subroutine jdot_mb_routine(binary_id , ierr)
    integer , intent(in) :: binary_id
    integer , intent(out) :: ierr
    integer :: k, nz
    type (binary_info), pointer :: b
    type (star_info), pointer :: s
    real(dp) :: turnover_time , envelope_edge
    real(dp) :: dr , tot_r , mb, jdot_mb
    real(dp) :: eta , wind_fac , saturate_fac
    real(dp) :: tt_boost , wind_boost
    real(dp) :: vel_ratio , tau_lim
    real(dp) :: rsun4 , two_pi_div_p3 , rad4
    ierr = 0
    call binary_ptr(binary_id , b, ierr)
    if (ierr /= 0) then
        write(*,*) 'failed_in_binary_ptr'

```

```

        return
    end if

s => b% s_donor
nz = s% nz
eta = s% x_ctrl(1)
wind_fac = s% x_ctrl(2)
vel_ratio = s% x_ctrl(3)
tau_lim = s% x_ctrl(4)
saturate_fac = s% x_ctrl(5)

tot_r = 0.0
turnover_time = 0.0
envelope_edge = 0.0
envelope_edge = max(s% conv_mx1_bot_r , s% conv_mx2_bot_r)

do k = nz , 1, -1
    if (s% mixing_type(k) == convective_mixing) then
        if ( s% r(k) .gt. envelope_edge) then
            if (k < s% nz) then
                dr = (s% r(k) - s% r(k + 1))
            else
                dr = (s% r(k) - s% R_center)
            end if
            if (s% conv_vel(k) .gt. vel_ratio * s% csound(k)
                .and. s% tau(k) .gt. tau_lim) then
                turnover_time = turnover_time + (dr/s% conv_vel(k))
                tot_r = tot_r + dr
            end if
        else
            turnover_time = turnover_time
        end if
    end if
end do

```

```

    tot_r = tot_r + dr
end if
end if
end do

! b% jdot_mb = 0
rsun4 = rsun*rsun*rsun*rsun
two_pi_div_p3 = (2.0*pi/b% period)*(2.0*pi/b% period)*&
(2.0*pi/b% period)

mb = -3.8d-30*b% m(b% d_i)*rsun4* &
pow_cr(min(b% r(b% d_i),b% rl(b% d_i))/rsun,
b% magnetic_braking_gamma)* &
two_pi_div_p3

! use the formula from rappaport, verbunt, and joss.
! apj, 275, 713-731. 1983.
if (b% have_radiative_core(b% d_i) .or. b% keep_mb_on) &

! 2.8d6 is turnover time in seconds for a MESA
! model using initial mass of 1.0 solar masses,
! solar metalicity, at age 4.6 Gyr. This is
! approximately turnover time of the Sun.

wind_boost = (b% mdot_system_wind(b% d_i) / (-1.6d12)) ** wind_fac
tt_boost = (turnover_time / 2.8d6) ** eta

jdot_mb = (wind_boost) * (tt_boost) * mb

! taking the period of the sun to be 24 days
! => 10 * P < Psun, P < 2.4 days

```

```

! 2.4 days = 207360 seconds

if (b% period < 207360) then

    ! use the formula from Ivanova & Taam 2003 for quickly rotating stars
    rad4 = b% r(b% d_i) * b% r(b% d_i) * b% r(b% d_i) * b% r(b% d_i)
    b% jdot_mb = (-6.0d30 * rad4 / rsun4) * 10 ** (1.7) * &
                  (2073600 / b% period) ** saturate_fac) * &
                  tt_boost * wind_boost

else
    b% jdot_mb = jdot_mb
end if

if (b% evolve_both_stars .and. b% include_accretor_mb .and. &
    (b% have_radiative_core(b% a_i) .or. b% keep_mb_on)) then
    b% jdot_mb = b% jdot_mb - &
                  3.8d-30*b% m(b% a_i)*rsun4* &
                  pow_cr(min(b% r(b% a_i),b% rl(b% a_i))/rsun,
                  b% magnetic_braking_gamma)* &
                  two_pi_div_p3
end if

end subroutine jdot_mb_routine

```

Appendix B

Sample MESA `inlist` Files

Simulations within `MESA` are run with `inlist` files, these files are read sequentially. If a variable is used multiple times, every subsequent use of the variable overwrites the previous input. The sample `inlist` files shown here are examples of uses from within the main body of the text. All parameters not listed in the sample `inlist` use the `MESA` default values.

B.1 Relaxation Sample

Forcing `MESA` to small time steps has the potential to introduce oscillations in the simulation that are purely numeric. At the same time a large time step has the potential to smooth over physical oscillations. In both cases the choice of time step has the potential of leading to unphysical results and the “best” choice of step size is not clear. In the case where the user wishes to force `MESA` from a large time step to very short time steps between two evolutionary points, a relaxation period is required to improve convergence of the simulation.

`&star_job`

```
! set MESA directory, if empty load using $MESA_DIR
mesa_dir = ''
```

```

! If empty use default from within $MESA_DIR/star/defaults
history_columns_file = ''
profile_columns_file = ''

! start a run from a saved model
load_saved_model = .true.
saved_model_name = FILE_TO_LOAD

! save a model once run is over
save_model_when_terminate = .true.
save_model_filename = FILE_TO_SAVE

! setting initial model number
set_initial_model_number = .true.
initial_model_number = 0

! force MESA to use a small dt
set_initial_dt = .true.
years_for_initial_dt = SMALL_DT

/ !end of star_job namelist

```

&controls

```

! maximum number of profiles, if negative no limit
max_num_profile_models = -1

! profile intervals, as we are trying to force small timesteps
! the profile and history output are not important
profile_interval = 10000

```

```
history_interval = 1000

! when to stop
! max model number, need to set a sufficiently large number
! of models to ensure that the model has ‘‘relaxed’’
max_model_number = LARGE_NUMBER

! max timestep size
max_years_for_timestep = SMALL_DT

/! end of controls namelist
```